Master's thesis

NTNU
Norwegian University of Science and Technology
Faculty of Engineering
Department of Mechanical and Industrial Engineering

Torbjørn Laastad and Even Renolen Litlabø

Virtual Crash Testing of a Frangible Aluminum Highway Gantry

Master's thesis in Mechanical Engineering
Supervisor: Terje Rølvåg
June 2019

NTNU
Norwegian University of
Science and Technology

Torbjørn Laastad and Even Renolen Litlabø

Virtual Crash Testing of a Frangible Aluminum Highway Gantry

Master's thesis in Mechanical Engineering
Supervisor: Terje Rølvåg
June 2019

Norwegian University of Science and Technology
Faculty of Engineering
Department of Mechanical and Industrial Engineering

NTNU
Norwegian University of
Science and Technology

Preface

This master thesis was submitted to the Norwegian University of Science and Technology (NTNU) in the spring of 2019. The work has been carried out at the Department of Mechanical and Industrial Engineering under the supervision of professor Terje Rølvåg.

The main part of this thesis is written as a scientific paper and submitted to the International Journal of Crashworthiness. The second part is presented in the appendix and consists of additional model information and complementary results.

We want to thank our supervisor professor Terje Rølvåg for providing invaluable assistance and equipment during this master period. Two computers were provided for the simulations as well as hard drives for the storage of result files. We were always welcome to visit his office with any questions or issues with the FEA model. Thanks are also given to Lattix, especially Tore Tøndevoll and Sören Ulonska for insight on the construction of Lattix gantries and test reports from their products.

Abstract

Traditionally, full-scale crash testing is performed to assess the passive safety performance of road-side structures. This thesis presents virtual crash testing of a Lattix 4438 highway gantry in accordance with EN12767. Lattix is a Norwegian company producing and developing frangible aluminum masts for aviation and road traffic. The objective was to determine if the gantry could be classified as non-energy absorbing. Simulations were performed in Abaqus Explicit, based on a detailed FE assembly model including all relevant structural components, contacts, boundary conditions, and bolt connections. The Norwegian Public Road Administration supplied the vehicle model used in the simulations. Acceleration and velocity data were extracted from the simulations for calculating Acceleration Severity Index (ASI) and Theoretical Head Impact Velocity (THIV). These parameters are indicators of the potential occupant injury during a crash.

The ASI and THIV values for the gantry fulfill the EN12767 requirements for a non-energy absorbing structure with designation 100NE2. The sampling rate was found critical for the accuracy of ASI values, and a sampling rate of minimum 40 kHz is recommended. Simulations show that the fracture load of the base bolts has a larger impact on ASI than the connection between leg and transom. Torsion of the transom may be an issue and should be investigated further. This was not investigated in this thesis due to the high simulation times (41h for 0.275 s simulated time). Non-linear static wind load analyses were performed, proving that the gantry survives a WL5 wind load category for single center mast configurations and WL7 wind load category for double center mast configuration.

Sammendrag

Tradisjonelt utføres fullskala kollisjonstesting for å vurdere sikkerhetsytelsen av ettergivende konstruksjoner for veiutstyr. Denne oppgaven presenterer virtuell kollisjonstesting av en Lattix 4438 trafikkportal utført i samsvar med EN12767. Lattix er et norsk selskap som produserer og utvikler ettergivende aluminiumsmaster for luftfart og veitrafikk. Det var ønskelig å avgjøre om portalen kunne klassifiseres som ikke-energiabsorberende. Simuleringene ble utført i Abaqus eksplisit, basert på en detaljert FE-modell, som inkluderer alle relevante strukturelle komponenter, kontakter, grensebetingelser og boltforbindelser. Statens vegvesen supplerte kjøretøysmodellen som ble brukt i simuleringene. Akselerasjons- og hastighetsdata ble hentet ut fra simuleringene for beregning av Acceleration Severity Index (ASI) og Theoretical Head Impact Velocity (THIV). Disse parametrene er indikatorer for potensiell personskade under en krasj.

ASI- og THIV-verdiene til portalen oppfyller kravene fra EN12767 for en ikke-energiabsorberende struktur med betegnelse 100NE2. Samplingsraten ble vist å være kritisk for nøyaktigheten av ASI-verdier, og en samplingsrate på minimum 40 kHz anbefales. Simuleringer viser at bruddlasten til baseboltene har større innvirkning på ASI enn forbindelsen mellom ben og tverrliggeren. Torsjon i tverrliggeren kan være et problem og bør undersøkes videre. Dette ble ikke undersøkt i denne oppgaven grunnet høye simuleringstider (41h for 0,275 s) simulert tid). Ikke-lineære statiske analyser ble utført, noe som viste at portalen overlever en WL5 vindlastkategori for portal med en sentermast og WL7 vindlastkategori for to sentermaster.

Contents

List of Figures

List of Tables

Abbreviations

$\overline{a}_n$ Average acceleration in n-direction

$\widehat{a}_n$ Limit acceleration value in n-direction

ASI Acceleration Severity Index

CoG Centre of Gravity

FEA Finite Element Analysis

t_n Time for current time step

t_{n-1} Time for previous time step

$THIV$ Theoretical Head Impact Velocity

v_n^{rel} Relative speed for current time step

v_{n-1}^{rel} Relative velocity for previous time step

WL Wind load

Introduction

For this master thesis, the authors and the supervisor agreed upon writing the thesis as a scientific paper. This paper was sent to the International Journal of Crashworthiness. It was further agreed on building the structure of the master thesis report around this paper; an introduction, then the paper itself, before extensive model information and complementary results presented in the Appendix. This master thesis is a continuation of the pre-project "Virtual Crash Testing of Traffic Portals" conducted between August and December of 2018.

A more in-depth introduction to what was done during the course of this project is given in the paper introduction.

Virtual Crash Testing of a Frangible Aluminum Highway Gantry

Even Renolen Litlabø*, Torbjørn Laastad† and Terje Rølvåg
Department of Mechanical and Industrial Engineering, NTNU

2019
June

Abstract

Traditionally, full-scale crash testing is performed to assess the passive safety performance of roadside structures. This paper presents virtual crash testing of a Lattix 4438 highway gantry in accordance with EN12767. Simulations were run in Abaqus explicit, based on a detailed FE assembly model. Acceleration and velocity data were extracted from the simulations for calculating Acceleration Severity Index (ASI) and Theoretical Head Impact Velocity (THIV). These parameters are indicators of the potential occupant injury during crash.

ASI and THIV values fulfill the EN12767 requirements for a non-energy absorbing structure with designation 100NE2. The sampling rate was found critical for the accuracy of ASI values, and a sampling rate of minimum 40 kHz is recommended. Simulations show that fracture load of the base bolts has a larger impact on ASI than the connection between leg and transom. Non-linear static analyses were performed, indicating that the gantry survives a wind load corresponding to at least WL2.

Keywords: *Crash simulation, FEA, Passive safety, ASI, THIV, Abaqus explicit*

*Contributed equally to this work with Torbjørn Laastad
†Contributed equally to this work with Even Renolen Litlabø

1 Introduction

This paper presents the results from the master thesis "Virtual Crash Testing of a Frangible Aluminium Highway Gantry". The goal of the performed work presented herein was to analyze if the gantry can be classified as a non-energy absorbing structure according to relevant standards. The work is based on Norwegian conditions and regulations.

The use of non-energy absorbing structures instead of the more traditional rigid structures can prevent severe injuries and possible death. Guard railing is used to stop vehicles from hitting rigid structures since an impact with such a structure may prove lethal. The problem with traditional guard railing is that vehicles can rebound into traffic, possibly causing secondary accidents. For crash with a non-energy absorbing structure, the vehicle continues its motion through the structure and comes to a halt at the roadside, minimizing the risk of further accidents.

Full-scale crash testing has been the traditional way of testing roadside structures. The objective of the physical tests is to verify that the structure passes the ASI and THIV requirements outlined in EN12767 for European regulations. For the physical testing, the behavior of the vehicle, accelerometer response, and injury potential are the evaluating factors. It is believed that the same results can be obtained by using explicit simulations. This will reduce the need for physical testing resulting in a reduction in cost for both development and testing of different structures. Previous use of FEA both on-road safety [3, 4, 5] and aviation masts [6] indicate that dynamic explicit finite element solvers can be utilized to recreate results from full-scale testing realistically.

By being able to test the structures in-house using virtual crash testing, it is considerably easier to perform more tests and to experiment with different solutions without the need to travel to a test track and set up a physical crash test. In Norway, there are currently no test tracks approved for these tests and hence, all testing must be performed abroad at significant cost and time demand.

The Norwegian company Lattix aims for delivering a non-energy absorbing gantries, and it is such a structure that has been analyzed in this paper. Their gantry consists of detachable sections of a highly deformable aluminum lattice structure. The purpose of the gantry is to hold informational signs, cameras, and open road tolling systems. An example of a Lattix gantry is shown in figure 1

Figure 1: Example of a Lattix gantry with three legs [1].

This paper is organized into sections describing the requirements, model, and simulations, before presenting the results, discussion, and conclusion. The requirements section goes into depth on criteria set forth to have a structure approved as non-energy absorbing. The next section describes the models used in the crash and wind load simulations. Details on how the simulations were configured are given in the simulation section. In the last three chapters, the results are first presented, then discussed before a conclusion is drawn.

2 Requirements

2.1 Crash

For the structure to be classified as a non-energy absorbing structure it has to fulfill the requirements of the following standards:

- NS-EN 12767 Passive safety of support structures for road equipment
- NS-EN 1317-1 Road restraint systems part 1

Acceleration Severity Index (ASI) and Theoretical Head Impact Velocity (THIV) are the main parameters defined in the standards for assessing accident severity.

ASI is a nondimensional quantity used as an assessment of accident severity for occupants of the impacting vehicle [7]. The peak ASI value during impact has been shown to be a good indicator of occupant injury [8, 9]. ASI value is calculated in accordance with EN1317-1, using equation (1) and (2) which uses accelerations in the three orthogonal directions. $\overline{a}_n$ is the component of the acceleration in the given direction averaged over a moving 50 milliseconds time interval while $\widehat{a}_n$ is the limit accelerations in the given directions. The typically used limit accelerations for passengers wearing seat belts are given in equation (3) [2].

$$ASI = max[ASI(t)] \tag{1}$$

$$ASI(t) = \left[\left(\frac{\overline{a}_x}{\widehat{a}_x}\right)^2 + \left(\frac{\overline{a}_y}{\widehat{a}_y}\right)^2 + \left(\frac{\overline{a}_z}{\widehat{a}_z}\right)^2\right]^{0.5} \tag{2}$$

$$\widehat{a}_x = 12g, \widehat{a}_y = 9g, \widehat{a}_z = 10g \tag{3}$$

THIV is the theoretical velocity at which a "point mass" occupant impacts the hypothetical occupant compartment [2]. When calculating THIV, the heads of occupants are considered as free objects, and its relative velocity compared to the vehicle is calculated. The vehicle is assumed to be moving in only one plane, meaning rolling is discarded. By using the midpoint rule, the distance the head has traveled relative to the vehicle can be calculated using equation (4). In the equation, v_n^{rel} is the relative velocity of the head for the current time step, v_{n-1}^{rel} is relative velocity for the previous time step, t_n is time passed up to the current time step and t_{n-1} is time passed to the previous time step. It was decided to use the midpoint rule with velocity instead of

the acceleration method that is being used in the standard because of the availability of accurate velocity data from the simulations, simplifying the process. The distance the head has traveled when hitting the dashboard of the vehicle is 0.6 m in the direction of the movement (x direction), or 0.3 m lateral from vehicle center line [2]. As the crash is head on, x is considered the critical direction. THIV is the velocity at which the head hits the dashboard.

$$x = \sum_{0}^{n} (\frac{v_n^{rel} + v_{n-1}^{rel}}{2}) * (t_n - t_{n-1}) \tag{4}$$

The structure shall be assessed based on three main criteria: speed class, energy absorption category (figure 2), and occupant safety level. Based on the performance of the structure it receives a designation, which is a combination of the performance on these three criteria. For example: a structure with a speed class of 100 km/h, energy absorption category of non-energy absorbing, and occupant safety level 2 gets the designation 100NE2. The designation criteria are shown in table 1 [7].

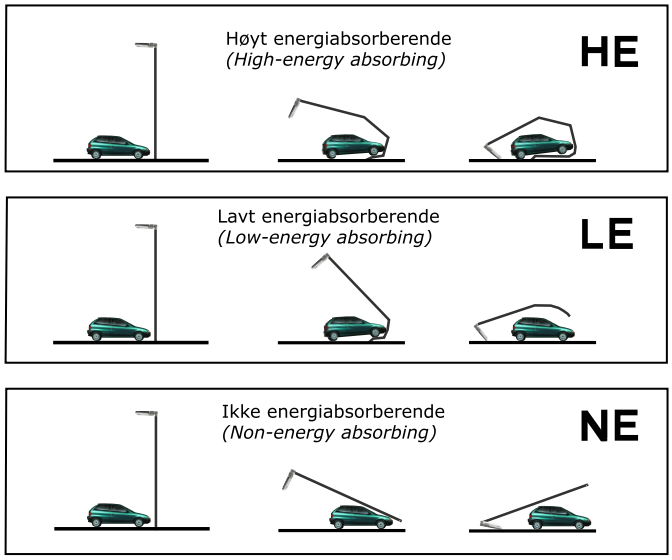

Figure 2: Energy absorption categories

Table 1: Occupant safety

Energy absorption categories	Occupant safety level	Speed			
		Mandatory low speed impact test $35 km/h$ Maximum values		Speed class impact test 50, 70, $100 km/h$ Maximum values	
		ASI	THIV km/h	ASI	THIV km/h
HE	1	1.0	27	1.4	44
HE	2	1.0	27	1.2	33
HE	3	1.0	27	1.0	27
LE	1	1.0	27	1.4	44
LE	2	1.0	27	1.2	33
LE	3	1.0	27	1.0	27
NE	1	1.0	27	1.2	33
NE	2	1.0	27	1.0	27
NE	3	0.6	11	0.6	11

The EN12767 standard requires two crash tests to be performed; one mandatory low-speed impact test at 35 km/h, and one at 50/70/100 km/h depending on which speed class the manufacturer chooses. In this case, the selected speed class is 100 km/h. ASI and THIV values must not, for any of the two tests, exceed 1.0 and 27 km/h respectively to be classified as a non-energy absorbing structure with occupant safety level 2. Additionally, the exit velocity of the 100 km/h test must be higher than 70 km/h. Finally, for cantilever and gantry type sign supports, the lowest point of the structure including signs must not be lower than 4 m for 15 minutes after the crash. This last requirement was not studied in this paper due to computational limitations.

This paper applies the ASI calculation method as described in the standard EN1317-1:1998, i.e. not EN1317:2010. The difference is that in 1998 the accelerations in the X, Y and Z directions are averaged over a moving 50ms interval, while the 2010 method instead introduces the use of a phaseless Butterworth filter. The filter is implemented to reduce the scatter of results by reducing the sensitivity to the vibrations of the accelerometer mounting [2]. Since the accelerations in the simulation are collected directly from a node, these vibrations are not an issue. The 2010 method also requires the collection of an additional 500 ms of data at the beginning and at the end of the main data. The 500 ms are needed because recursive filters produce starting transients that need time to "settle down" [2]. Collection of 500 ms pre and post crash data would greatly increase the already long simulation time (about 41 hours for 275ms simulated time). This does not mean that the data is not filtered as the 50 ms moving average in equation (2) acts as a low pass filter. By filtering the raw data the highest frequencies of accelerations can not pass, taking into account the fact that vehicle accelerations are transmitted to the occupant bodies through relatively soft contacts [10].

The accelerations are extracted from a node near the center of gravity [2]. In order to further reduce the high frequency vibrations, a small mass was added to the node, which acts to numerically smooth the data [11].

2.2 Wind load

For environmental loads the following standards apply:

- NS-EN 12899-1 Fixed, vertical road traffic signs
- NS-EN 1991-1-4 Eurocode 1: Actions on structures

The structure should be able to withstand environmental loads that it is expected to be exposed to. Wind is the dominating environmental load for this type of gantry. This wind load is estimated using EN1991-1-4 (Eurocode 1) and HB R310 (The Norwegian Public Roads Administration). Several factors influence the wind load, such as height, geometry, topography, and geographic location. Wind load are categorized according to EN12899, from WL1 to WL9 equivalent to a wind load of 0 to 1600 N/m^2 respectively.

The requirements with regards to wind load depends on installation site, which has not been defined. Data on wind load are supplied by Lattix through an Excel document following relevant standards [12, 13].

2.3 Vehicle

The EN1317-1 standard specifies the characteristics and dimensions that the test vehicle must comply to. These are presented in table 2 along with the dimensions and characteristics of the FEA model. The model used in this paper is a Geo Metro compact model supplied by the Norwegian Public Road Administration.

Table 2: Vehicle specifications [2]

Parameter		GM Compact	Standard
Total Mass	$[kg]$	888	900±40
Test inertial mass	$[kg]$	813	825±40
Wheel Track	$[m]$	1.39(front) 1.33(rear)	1.35±20
Center of Gravity			
Longitudinal distance from front axle		0.89	0.90±0.09
Lateral distance from vehicle center line	$[m]$	0.02	0±0.07
Height above ground		0.47	0.49±0.05

3 Model

3.1 Simplified crash model

A simplified model of the gantry was used to reduce simulation time and storage space requirements for the sensitivity analyses. The simplified model consists of the vehicle model and the simplified 4438 Lattix gantry assembly. Most of the gantry is modelled using 1D beam elements, only the leg that is crashed into is modeled using solid elements as shown in figure 3. The solid elements are connected to the beam elements using a wire connector. The vehicle hits the gantry at a 20° angle.

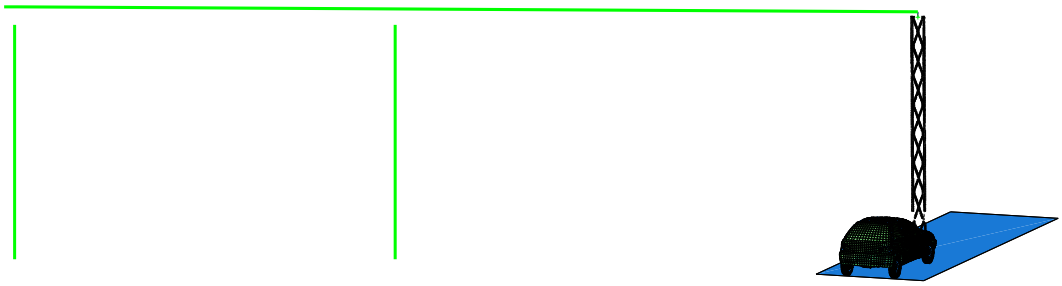

Figure 3: Simplified model

3.2 Crash model

For the full model, Lattix 4438 mast sections replace all beam elements in the simplified model, and the top wire connector is replaced with a connection designed to fail in shear to make the model as close to real-life as possible. The model is shown with measurements and impact point of the vehicle in figure 4. The different mesh elements used in different parts of the model are presented in table 3.

Table 3: Mesh data for the model

Part	Element type	Order	Size $[mm]$
Vehicle	S4R S3R C3D8R	Linear	18-77
4438 Mast	C3D8R	Linear	12
Base plate	C3D8R	Linear	10
Bracket	C3	Linear	12
Sign	S4R	Linear	20

Regular M10 bolts are used at the top connection and notched M14 bolts for the base connection. The M14 bolts are made with two bolt parts and a wire connector between them to simulate the

fraction section of the bolt. It is assumed that the simplification will have a negligible impact on the result.

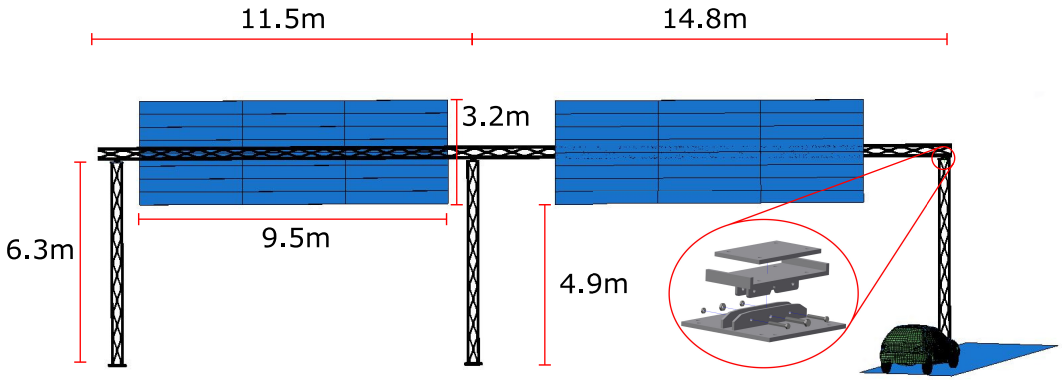

Figure 4: Full crash model

3.3 Wind model

For the non-linear static simulations used for wind load, the vehicle was removed from the model leaving only the gantry. The signs on the gantry are placed symmetrically about the center axis of the transom of the gantry [7].

3.4 Materials

The material used for the 4438 mast sections is 6063F25-T66 aluminum. The base plate connecting the mast to the ground is made from S355J2G3 steel, while the Bumax 109 bolts are made from AISI 316L stainless steel. The vehicle model consists of more than 200 different materials that were imported from the provided model and will therefore not be covered here. Material properties are presented in table 4.

Table 4: Material properties used in the model.

Material	Youngs's modulus $[GPa]$	Poisson's ratio	Density $[Kg/m^3]$	Thermal expansion coefficient K^{-1}	Fracture strain	Yield point 1 (stress, strain) $[MPa, -]$	Yield point 2 (stress, strain) $[MPa, -]$	Yield point 3 (stress, strain) $[MPa, -]$
Aluminum 6063F25-T66	70	0.33	2700	N/A	0.3	239 0	268.9 0.107	N/A
Steel S355J2G3	210	0.3	7850	$1.1 * 10^{-5}$	1	355 0	N/A	N/A
AISI 316L	210	0.3	7800	$1.1 * 10^{-5}$	0.078	1100 0	1674 0.011	1910 0.127

4 The simulations

Two different types of simulations were performed; dynamic explicit crash simulations, and non-linear static wind load simulations.

4.1 Sampling rate sensitivity analysis

Previous studies have shown that ASI values are sensitive to sampling rates [14]. Because of this, a sampling rate sensitivity analysis was conducted using the simplified model with a velocity of 100 km/h. This was accomplished using one identical model for several simulations, only altering the sampling rate. Results obtained from the simplified model are assumed to translate well over to the full model.

The analysis consists of the four first steps in table 5. The different steps are used to apply loads and boundary conditions to represent the physical testing of the mast. "Moving Average" is used to ensure the ASI peak value is obtained. A difference in temperature is used to create pretension in the bolts connecting the mast to the base plate.

4.2 Sensitivity to base bolt fracture load

Because of the geometry of the gantry, it was assumed that the fracture load of the base bolts have a significant impact on ASI values. A sensitivity analysis was conducted using the simplified model where only the fracture load of the base bolts was changed. An impact velocity of 100 km/h was used for the simulations. As ASI is assumed to be more sensitive than THIV to the fracture load of the base bolts, only the first four steps are used for this sensitivity analysis.

4.3 Crash

For the full simulation, the first four steps are identical to the simplified simulation and a final step was implemented. The last step, "After crash", is 200 ms bringing total time from when the vehicle first meets the mast to end of simulation to 275 ms. This step is 200 ms because this is the time it takes for the head to travel the necessary 0.6 m to allow for the calculation of THIV. By using a 40 kHz sampling rate only where ASI value is obtained, the size of the result file is reduced. All five steps are presented in table 5.

Table 5: Steps summary for full model simulation

Step	Duration $[s]$	Start time $[s]$	End time $[s]$	BC	Interactions	Load	Predefined fields	Sampling rate $[kHz]$
Initial	0	0	0	Fixed plate Fixed road Fixed mast	General contact	N/A	Temp ref. Temp bolts Initial velocity	N/A
Pretension	0.0001	0	0.0001	Propagated	Propagated	Gravity, Rolling resistance	Pretension, Temp. Bolts, Propagated	20
Crash	0.05	0.0001	0.0501	Propagated	Propagated	Propagated	Propagated	40
Moving Average	0.025	0.0501	0.0751	Propagated	Propagated	Propagated	Propagated	40
After crash	0.20	0.0751	0.2751	Propagated	Propagated	Propagated	Propagated	10

4.4 Wind load

For the wind load simulations, a static non-linear solver was used. A linear ramp up pressure load of 1.6 kN/m^2 was applied normal to the signs. This pressure translates to a total of 97.28 kN applied to the transom.

5 Results

5.1 Sampling rate sensitivity

The initial sampling rate of 10 kHz gave ASI values that were inconsistent and erroneous. There was no apparent correlation between an increase in fracture load of the top connector and ASI value, as shown in figure 5a. Based on these results, several simulations with a higher sampling rate were conducted. First, a simulation with a sampling rate of 536.4 kHz (the highest possible sampling rate with available storage) was conducted. When comparing the raw acceleration data from 10 kHz and 536.4 kHz, it is clear that the 10 kHz sampling rate is jagged, while the 536.4 kHz is smooth as shown in figure 6. It is evident that the lower sampling rate is unable to capture accurate acceleration data.

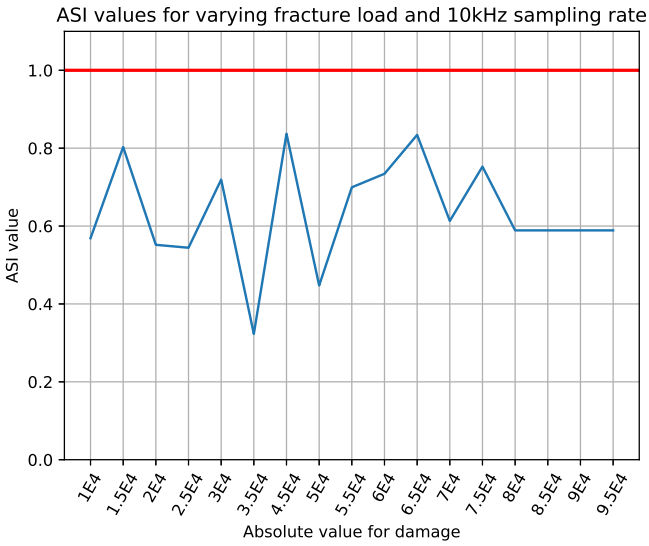

(a) ASI value for $10kHz$ sampling rate

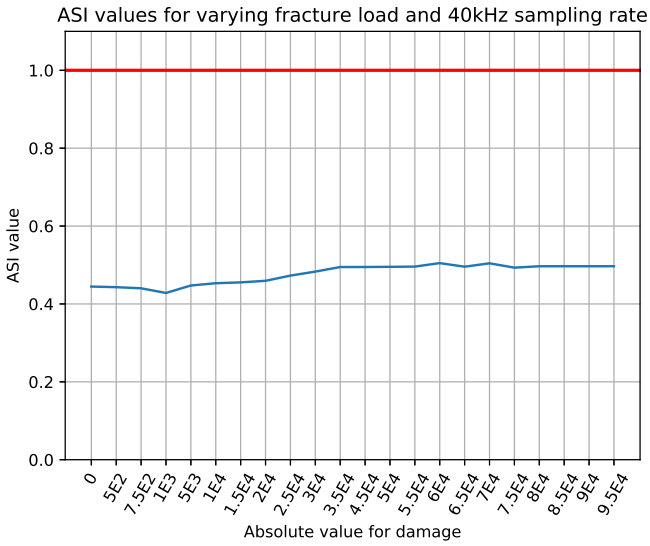

(b) ASI value for $40kHz$ sampling rate

Figure 5: Comparison between simulations with $10kHz$ and $40kHz$ sampling rate

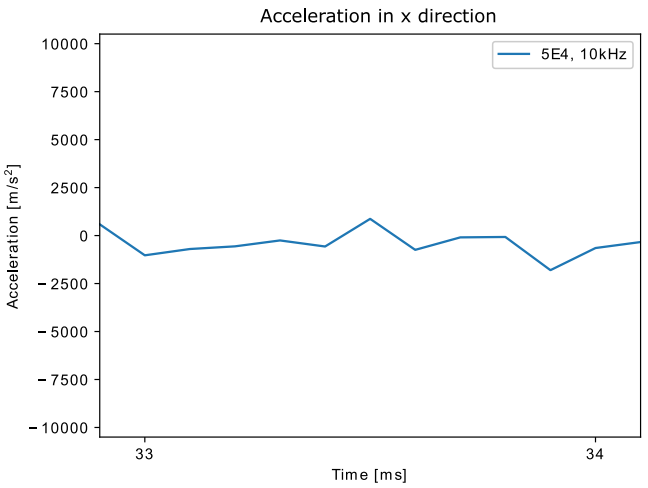

(a) Raw data for $10kHz$ sampling rate

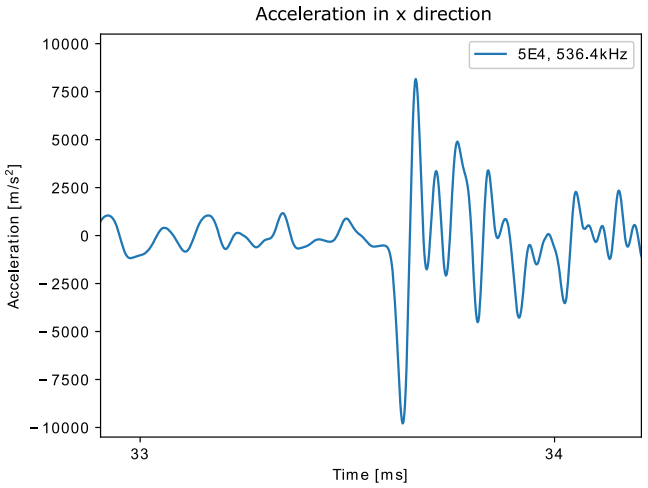

(b) Raw data for $536kHz$ sampling rate

Figure 6: $10kHz$ and $536.4kHz$ sampling rate

The ASI value for the 536.4 kHz sampling rate was used as a reference value for all simulations in the sensitivity analysis to determine a sampling rate with an acceptable trade-off between result file size and accuracy. The results from the sensitivity analysis are shown in table 6.

Table 6: Result of sensitivity analysis

Sampling rate $[kHz]$	ASI value	Deviation [%]	File size $[Gb]$
536.4	0.495	-	600.0
2	1.085	119	2.4
5	1.795	263	5.7
10	0.925	87	11.3
20	0.602	22	22.5
30	0.512	3	33.7
40	0.502	1.4	44.9
50	0.503	1.6	56.0
60	0.502	1.4	67.2
100	0.503	1.6	111.9

Sampling rates of 40 kHz and higher yield similar ASI values and have a sufficiently small deviation from the reference value, leading to the size of the result files becoming the deciding factor. Result files for full model including all steps is estimated to be 10 times larger than the ones presented in table 6. Based on this, a sampling rate of 40 kHz was chosen for all further crash simulations. Figure 5b shows the new sampling rate yields a predictable and credible curve for ASI.

The ASI values presented here are not directly comparable to those presented later in the paper. These ASI values were obtained using an earlier version of the model. The resulting sampling rate is still valid as all simulations in the sensitivity analysis were run on the same model and therefore directly comparable to each other.

5.2 Sensitivity to base bolt fracture load

The ASI value sensitivity to different fracture loads of the bottom bolts was investigated. As expected, the ASI values increase when the strength of the bolts increases, as shown in table 7 and figure 7.

Table 7: Fracture load vs. ASI

Fracture load $[kN]$	ASI
110	0.393
115	0.394
120	0.410
125	0.442
130	0.470
135	0.489
140	0.510
145	0.527
150	0.556
155	0.584
160	0.681
165	0.787

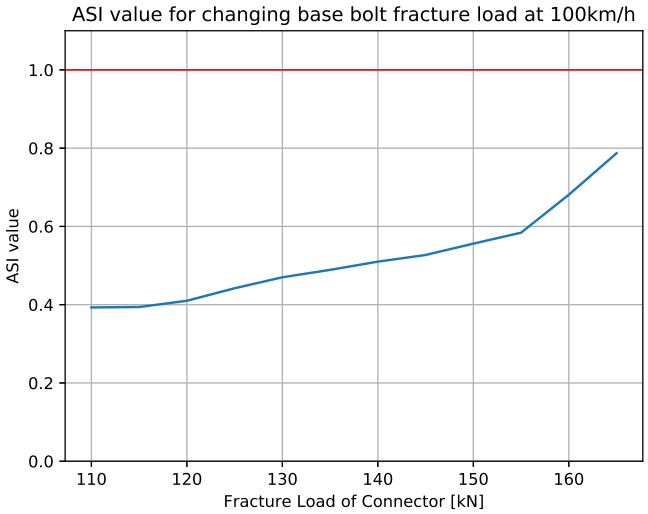

Figure 7: ASI plotted against fracture load of base bolts

The notched M14 Bumax 109 bolts used in the Lattix 4438 gantry were tested to a tensile load of 117 kN [15]; however, because of uncertainties in material behavior during high strain rates, a safety factor of 1.15 was applied. The resulting fracture load of 135 kN was used in all later simulations.

5.3 Crash simulation

Simulation run with the full model using 40 kHz sampling rate, a 135 kN fracture load for base bolts, and 22 kN fracture load for top connection bolts gave an ASI value of 0.56 for 35 km/h and 0.50 for 100 km/h. The THIV values were 18.1 and 10.1 km/h for 35 and 100 km/h respectively. All values are well within the criteria for being classified as a non-energy absorbing mast with occupant safety level 2. Figure 8 shows the final increment of the simulation, where the leg has detached from the base and transom.

The simulations revealed a potential issue with the torsion load in the transom. For the long transom section, the torsion load is 18.7 kNm, while for the shorter transom section, the torsion load is 14.4 kNm. These torsion loads are extracted from the end of the simulation which lasts 0.275 s, meaning the behavior of the transom after this point in time is unknown. The torsion capacity of the 4438 mast is 21 kNm [16] without material factors or factors of safety. For the long transom section a continued torsion may result in a torsion load exceeding the capacity.

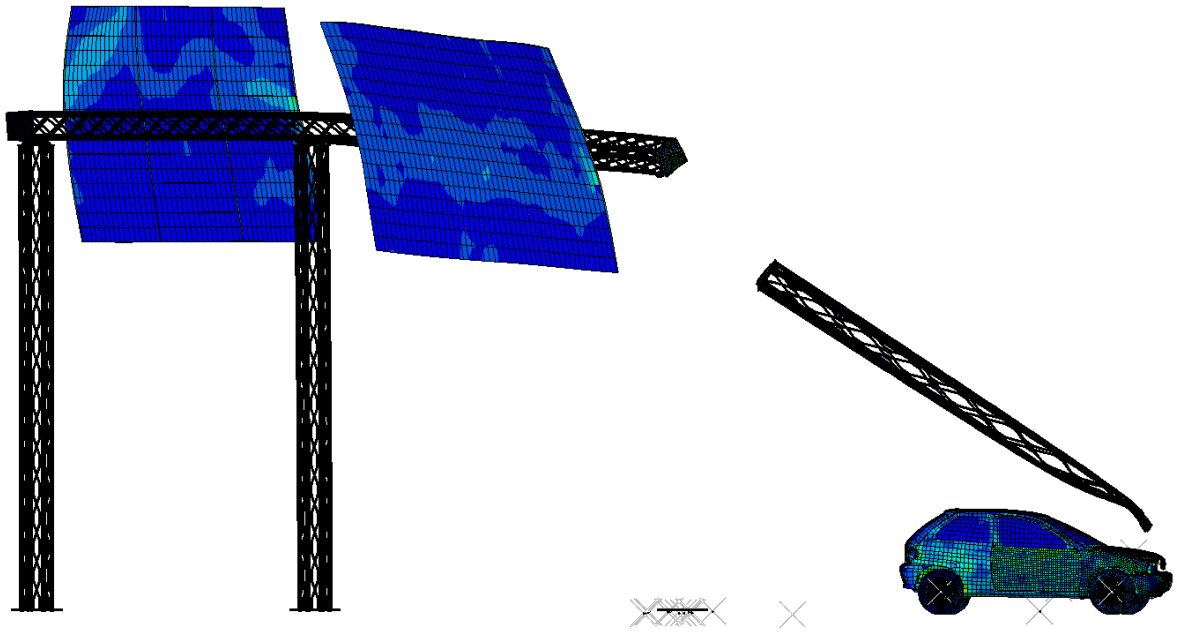

Figure 8: Final increment of crash simulation.

5.4 Wind load

Static non-linear simulations were performed for wind loads, with both one and two center masts. Based on the bending capacity of the masts, 152 kN [16], highest allowable wind pressure for this mast and sign size is 0.79 kN/m^2. The simulations, however, indicate that the gantry with one center mast can withstand loads up to 1.0 kN/m^2. At this load, the cross-section of the center mast starts to yield, as shown in figure 9 where stress in the gray areas is above the yield strength of 239 MPa. For both wind loads the relationship between applied load and displacement of the transom is still linear as shown in figure 10a. This indicates that the mast still retains it's structural integrity.

For the double center mast configuration the bending capacity results in a maximum wind load of $1.58kN/m^2$. This is higher than what was obtained from the simulations as the relationship between applied load and displacement stops being linear at 1.5 kN/m^2 after which severe yield occurs. Visual inspection of the cross section indicate a maximum load of 1.4 kN/m^2. The results from the wind load simulations and calculations indicate theat the gantry survives the required wind load for WL2 for the single center mast and WL7 for the double center mast configuration [17].

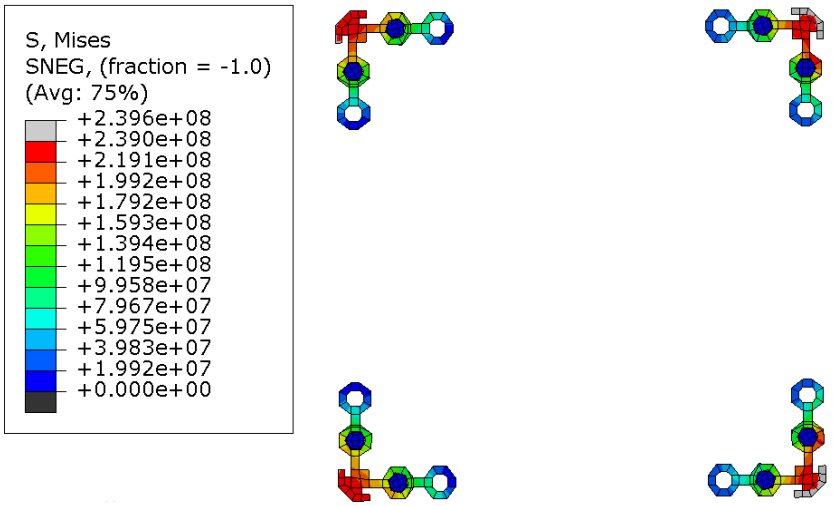

Figure 9: Stresses in center mast for single center mast configuration

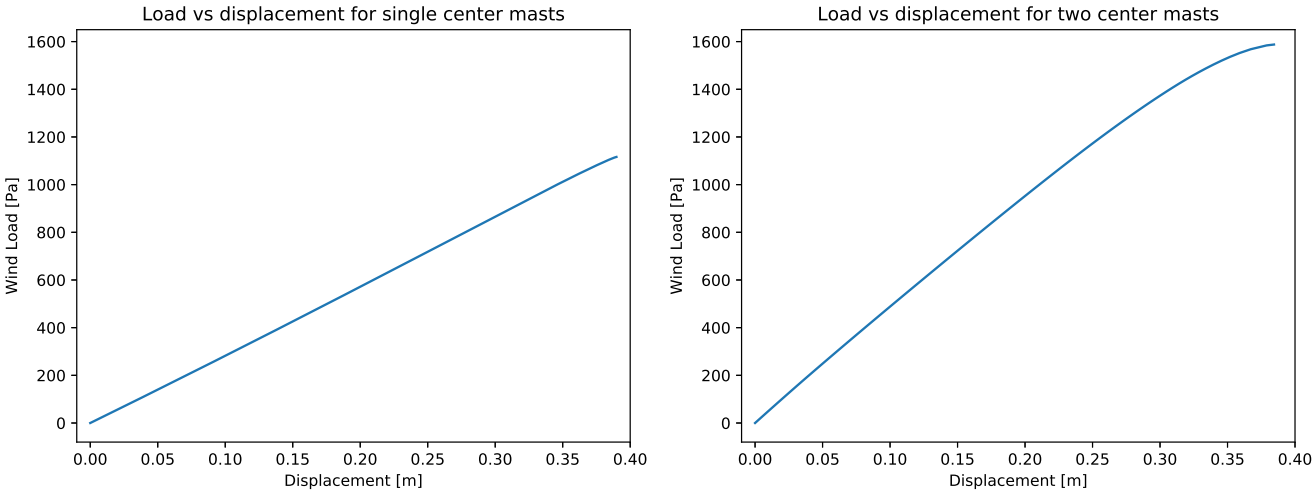

(a) Single mast configuration

(b) Double mast configuration

Figure 10: Applied wind load vs displacement of transom for both configurations.

6 Discussion

6.1 Sampling rate sensitivity

The sampling rate used in the simulations was proven to have a significant effect on the calculation of ASI values. When using a 10 kHz sampling rate, the data points are not close enough to accurately capture the acceleration data. This is clear when comparing raw acceleration data from 536.6 and 10 kHz. Not only are several peak values not captured with the lower sampling rate, but the resulting peak values for 10 kHz are significantly lower than for the higher sampling rate.

If accurate acceleration data is not obtained, there is a risk of approving a structure based on insufficient data. For the simulations presented in this paper, the ASI values are still below 1 even for the low sampling rate, but this could be critical if the values are close to the limit. Based on the findings presented a minimum sampling rate of 40 kHz should be used for this model. For other models, a sampling rate sensitivity analysis is recommended for complete confidence in the ASI results.

The THIV results have been consistent throughout the simulations and have not been affected by the sampling rate to the same degree as ASI values. This low variation is assumed to be caused by the high-frequency accelerations, which do not have a significant impact on the velocity of the vehicle.

6.2 Bolt Material

A simplification was done in the simulations by using a wire connector feature to represent the fracture section of the Bumax bolts. This connector does not account for the strain rate behavior of the bolt material. The fracture load of the connector is based on a tensile test of the Bumax bolts [15]. During the crash, the bolts connecting the mast to the base plate experience a high strain rate, which influence the material behavior of the bolts. Tests conducted on AISI 316L stainless steel show a significant strain rate dependency at high strain rates (1000 s^{-1} to 5000 s^{-1}) [18].

The Abaqus software has capabilities of handling strain rate dependent material data, either in tabular form or through the input of parameters to a material model such as the Johnson-Cook model. Several studies have tried to fit the test data of 316L in the annealed state by the use of Johnson-Cook model, obtaining widely varying parameters [19, 20]. Acquiring parameters that accurately reflect the strain rate behavior of the Bumax bolts would require testing of the same material at the level of work hardening and heat treatment of the Bumax bolts. Little work has been done in literature on the effects of work hardening and heat treatment on the strain rate behavior of 316L stainless steel, so a strain rate behavior model was not implemented in the simulations.

Implementing an accurate strain rate model would yield more realistic behavior of the bolts, further improving the results of the simulations. The bolts would fracture at different loads for

the 35 km/h and 100 km/h simulations because of the difference in strain rate. As the base bolt fracture strength sensitivity analysis showed, an increase in fracture strength would yield higher ASI values. However, even with strain rate behavior accurately modeled the fracture load of the bolts is assumed to not exceed the maximum load used in the analysis. This means that the gantry would still meet the requirement of an ASI value below 1.

6.3 Physical testing vs. Simulations

Physical testing of a single mast configuration was conducted by Lattix in 2006 [21]. At the time of the testing, notched M16 bolts was used to connect the mast to the base plate. Linear interpolation between 155 and 160 kN was used to estimate ASI for a fracture load of 157 kN, corresponding to the minimum fracture load of unnotched Bumax 109 M16 bolts [22]. This results in an ASI value of 0.62 which is lower than the ASI value obtained for physical testing 0.69. The physical tests were performed with a single roadside sign mast, meaning they are not necessarily comparable to a gantry crash simulation. Strain rate depedency, differences in test vehicles and instrumentation, fracture load, and geometrical differences are factors contributing to the difference between simulated and real-life values for ASI.

6.4 Base bolt fracture load

Because of the low impact point on the gantry leg, it is evident that the material properties of the bolts connecting the mast to the base plate have a more significant impact on ASI than the bolted connection at the top. One explanation for this could be that the top connector is subjected to large moment having a 6.3 m long vertical mast being deformed in combination with torsion of the 14.8 m transom. The transom acts as a torsion spring absorbing energy, resulting in the fracture load of the connection having a smaller impact than if no torsion was possible.

The distance between the impact point and lower bolts is considerably shorter than between impact point and top, with 0.5 m to base and 5.8 m to top. Because of the considerable smaller potential for deformation, the fracture load of the bolts becomes the controlling factor of the severity of the crash. The results of the base bolt sensitivity analysis clearly show that the lower bolt has a considerably higher effect on ASI than the top connection. For an increase in fracture load of 55 kN the increase in ASI was 0.39 for the base bolts. As shown in figure 5b, increasing the fracture load of the top connection by 95 kN only results in an increase in ASI of 0.076.

6.5 Transom torsion

The reason for the difference in torsion load between the short and long section has not been determined. However, it is assumed that because of the longer section allows for a larger angle, the mast induces a larger rotational velocity before the bracket is separated. The torsion is mainly caused by the bracket not failing early enough, and therefore the rotation of the gantry leg is transferred into the transom. The simulations are done in a complete vacuum, meaning the signs to some degree will reduce the rotation when air is introduced. However, the gantry is designed to hold informational signs as well as act as a toll booth gantry. For the toll booth, there are no

signs, meaning less effect of the resistance of air.

The performed simulations stop 0.275 s after impact. If the torsion continues, it could result in the transom falling lower than 4 m above the road and therefore not be approved as a non-energy absorbing structure. This was not further investigated here, but should be verified before final approval of the structure. Because the ASI and THIV values are well within the requirements, the resulting height above ground after a crash might be the determining factor for approval as a non-energy absorbing structure.

6.6 Wind simulations

The wind simulations show that the single center mast structure can withstand a wind load of 1 kN/m^2 for this particular sign configuration. At this point, the relationship between applied load and displacement of transom is linear, and the visual inspection indicates that the cross section is starting to yield. It is, however, difficult to determine at which point there is yield in such a large portion of the cross-section that it is a real threat to the structural integrity of the gantry. This is evident when comparing the result from simulations to the bending capacity calculations for the mast. The calculations indicate a maximum wind load of 0.79 kN/m^2 for the masts, meaning the estimate from the simulations is too high.

For the double center mast configurations this is not the case. Here the bending capacity results in a maximum wind load of 1.58 kN/m^2 while the estimate from the simulations indicate a maximum wind load of 1.4 kN/m^2. Based on these findings it is recommended to verify simulations with calculations and vice versa to ensure the structure survives the required wind load.

7 Conclusion

The results presented in this paper show that the Lattix 4438 gantry passes the criteria to be classified as a non-energy absorbing structure with regards to ASI and THIV as summarized in table 8. The gantry fulfills the ASI and THIV requirements to get a 100NE2 designation. There is, however, a torsion load in the transom that could be an issue. The torsion in the transom is shown to be close to the limit already after 0.275 s. It is unknown if this torsion increases further after the end of the simulations. If the torsion exceeds the capacity, the transom could fall below 4 m violating the height requirement, or worst case, the entire gantry could fail. The work on this thesis has revealed that the requirement of minimum resulting height above ground after a crash can be more critical for being classified as a non-energy absorbing structure than ASI and THIV.

Table 8: ASI and THIV result

Velocity $[km/h]$	ASI	ASI requirement	THIV $[km/h]$	THIV requirement	Exit velocity $[km/h]$
35	0.6	1.0	18	27	16.8
100	0.5	1.0	10	27	89.6

The ASI results were shown to be sensitive to the sampling rate of the simulation, and care should be taken to make sure no data is lost because of sampling issues. A sampling rate of at least 40 kHz is recommended.

Additionally, the fracture strength of the base bolts was shown to have a significant impact on the ASI values. This should be kept in mind when deciding what bolts to use for connecting the gantry legs to the base plate.

Results from the static wind simulation indicate that the single mast configuration can be classified as a WL5, however, calculations based on the bending capacity of the mast yield a classification of WL2. The double mast configuration can be classified as WL7 according to simulations and WL8 according to analytical calculations.

8 Further work

- For complete confidence in the simulation results, more extensive model validation should be performed by directly comparing acceleration data from a physical crash test to simulation data. The comparison of the acceleration data can be made for example with the Roadside Safety Verification and Validation Program (RSVVP) developed at the Worcester Polytechnic Institute [23].
- Failure of the shear bracket needs to be investigated further to ensure an acceptable torsion load in the transom. Further investigations is recommended to ensure meeting the requirement of necessary height above the road after a crash and to verify that the transom does stay intact[7].
- The vehicle model should be updated to a vehicle that is more representative of the current traffic in Europe.

9 Acknowledgements

The authors are grateful to Lattix, especially Tore Tøndevoll and Sören Ulonska, for sharing insight on the construction of Lattix gantries and test reports from their products.

10 Disclosure Statement

No potential conflict of interest was reported by the authors.

References

[1] Lattix. Gantry with 3 legs, 2019. https://www.lattix.net/product-page/lattix-gantry-with-3-legs. Accessed 26.05.2019.

[2] *Road restraint systems Part 1: Terminology and general criteria for test methods*, NS-EN 1317-1:2010, July 2010.

[3] Dhafer Marzougui, Cing-dao Kan, and Nabih E. Bedewi. Development and validation of an ncap simulation using ls-dyna3d. 12 1997.

[4] K. T. Gursel and S. N. Nane. Non-linear finite element analyses of automobiles and their elements in crashes. *International Journal of Crashworthiness*, 15(6):667–692, 2010.

[5] Wojciech Wach. Crash against mast according to en 12767 standard – uncertainty of passive safety indexes calculated in programs for simulation of vehicle accidents. Proceedings of the 21th Annual Congress of the European Association for Accident Research and Analysis (EVU), Braşov, Romania, 2012.

[6] Terje Rølvåg, Torgeir Welo, Rien van Houten, and Jaap Wiggenraad. Fe simulation of soft wing impactor for aviation mast frangibility testing - sensitivity to model assumptions. *International journal of crashworthiness*, 21:435–451, April 2016.

[7] *Passive safety of support structures for road equipment Requirements, classification and test methods*, NS-EN 12767:2007, November 2007.

[8] Douglas Gabauer and Hampton Gabler. Evaluation of threshold values of acceleration severity index by using event data recorder technology. *Transportation Research Record*, 1904(1):37–45, January 2005.

[9] Dr M Shojaati and Eth Zurich. Correlation between injury risk and impact severity index asi. 3rd Swiss Transport Research Conference, Monte Verità, Switzerland, 2003.

[10] *Road restraint systems Part 1: Terminology and general criteria for test methods*, NS-EN 1317-1:1998, April 1998.

[11] Edwin Fasanella and Karen Jackson. Best practices for crash modeling and simulation. November 2002.

[12] Norwegian Public Roads Administration. Traffikksikkerhetsutstyr Tekniske krav, 2011.

[13] *Eurocode 1: Actions on structures, Part 1-4: General actions, Wind actions*, NS-EN 1991-1-4:2005+NA:2009, April 2005.

[14] Terje Rølvåg. Crash simulations of the Lattix 4438 L11885 mast. May 2018.

[15] Teknologisk Institutt. Mechanical testing of threaded steel bolts. Oslo, Norway, 72932-05-023313, March, 2016.

[16] Research Institutes of Sweden AB. Stiffness bendig test of masts. Borås, Sweden, 7P07540 Rev.1, 27.11.2017.

[17] *Fixed, vertical road traffic signs - Part 1: Fixed signs*, NS-EN 12899-1:2007, March 2007.

[18] Woei-Shyan Lee, Tao-Hsing Chen, Chi-Feng Lin, and Wen-Zhen Luo. Dynamic mechanical response of biomedical 316l stainless steel as function of strain rate and temperature. *Bioinorganic chemistry and applications*, 2011, December 2011.

[19] D. Umbrello, R. M'Saoubi, and J.C. Outeiro. The influence of johnson–cook material constants on finite element simulation of machining of aisi 316l steel. *International Journal of Machine Tools and Manufacture*, 47(3):462 – 470, 2007.

[20] Nikolaos E. Karkalos and Angelos P. Markopoulos. Determination of johnson-cook material model parameters by an optimization approach using the fireworks algorithm. 11th International Conference Interdisciplinarity in Engineering, INTER-ENG 2017, 5-6 October 2017, Tirgu Mures, Romania, 2018.

[21] Nordic Test Center AS. Confirmation of certification testing 100km/h, December 2006.

[22] Bumax. Tightening torque and force, 2019. Accessed: 2019-05-02.

[23] Mario Mongiardini, Malcolm Howard Ray, and Marco Anghileri. Development of a software for the comparison of curves during the verification and validation of numerical models. 7th International LS-DYNA Conference, Salzburg, Austria, 2009.

[24] Torbjørn Laastad. Virtual Crash Testing of Traffic Portals. *Norwegian University of Science and Technology*, December 2018.

[25] SIMULA. Abaqus 2016 documentation.

A Detailed model information

Large portions of the information presented for the model, assembly, interactions and boundary conditions are previously presented in the project assignment "Virtual Crash Testing of Traffic Portals"[24]. This was a pre-project and the origin for the master thesis. All words in italic are Abaqus specific functions.

A.1 Models

The models consists of a simplified Geo Metro compact vehicle and the Lattix 4438 gantry. Two different models were used, a simplified model and a complete model. The simplified model was received from Terje Rølvåg with only the support leg that is being crashed into modeled in full, and the rest of the gantry represented by beam elements. For the complete model, all beam elements were replaced with mast sections and bolted connections. The complete model was used for both crash and wind load simulations.

A.1.1 Mast

A section of the Lattix 4438 mast used in this report is shown in figure 11, while the full mast assembly is described in chapter A.2.1. Mesh elements are linear 8-node brick elements with reduced integration (C3D8R) and a nominal size of 12 mm. To maintain a consistent mesh and keep a reasonably low simulation time a relatively coarse mesh was used. This results in the meshed part differing somewhat from the geometrical model. Small features like fillets are lost, and circles appear as more of a hexagonal. The material of the mast is 6063F25-T66 aluminum with properties displayed in table 9. The most relevant mechanical properties of the mast are a torsion capacity of 21 kNm, torsion stiffness of 11 $kNm/(°/m)$ and bending capacity of 152 kNm [16].

(a) Isometric view of mast

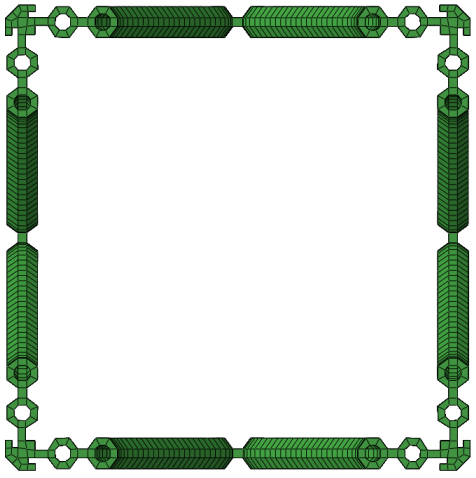

(b) Section view of mast

Figure 11: Lattix 4438 mast

Table 9: Material properties for 6063F25-T66 aluminum.

Material	Young's modulus $[GPa]$	Poisson's ratio	Density $[Kg/m^3]$	Thermal expansion coefficient K^{-1}	Fracture strain	Yield point 1 (stress, strain) $[MPa, -]$	Yield point 2 (stress, strain) $[MPa, -]$
Aluminum 6063F25 T66	70	0.33	2700	N/A	0.3	239 0	268.9 0.107

A.1.2 Base plate

The base plate connecting the mast to the foundation was meshed with 8-node linear brick elements with reduced integration (C3D8R) and nominal size of 10 mm. Because of the simple geometry of the base plate, the geometrical and meshed geometries match. Figure 12 shows the base plate while table 10 shows the material properties.

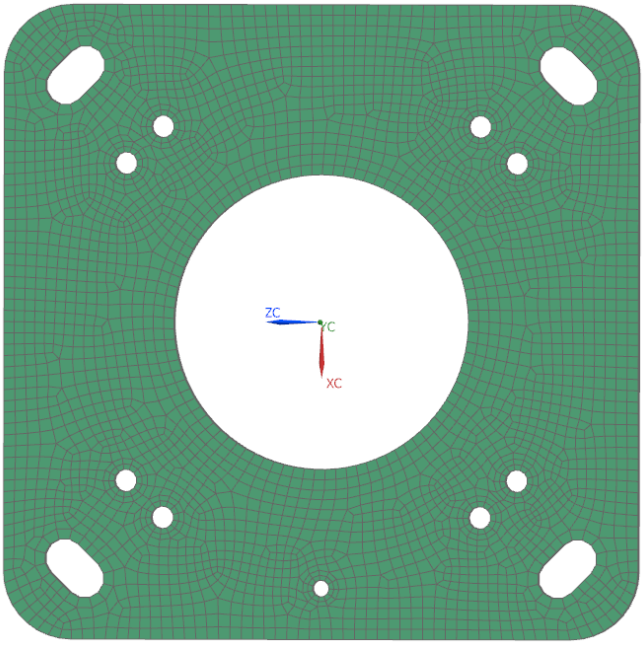

Figure 12: Base plate of the mast.

Table 10: Material data for S355J2G3 steel.

Material	Youngs's modulus $[GPa]$	Poisson's ratio	Density $[Kg/m^3]$	Thermal expansion coefficient K^{-1}	Fracture strain	Yield point 1 (stress, strain) $[MPa, -]$
Steel S355J2G3	210	0.3	7850	$1.1 * 10^{-5}$	1	355 0

A.1.3 Bolts and washers

The bolts connecting the base plate to the mast are Bumax 109 M14 bolts. Each bolt is modeled as two parts with a wire connector between them. This configuration will be explained more in-depth in section A.3.4 Bolts. The meshed geometry is what can be described as two hexagonal sections, one for the head and one for the shank of the bolt. The bolts are meshed with linear 8-node brick elements with reduced integration (C3D8R) and a nominal mesh size of 12 mm. The mesh size is too large to allow for a perfect representation of the geometrical model, but since the the mesh of the bolts is not critical, it is sufficient. Figure 13a shows the bolt viewed along the shank with the red circle representing the geometric model, and the black lines showing meshed geometry of the shank. It is clear that the meshed geometry, in black, does not perfectly represent the geometrical model.
The washers are meshed with linear 8-node linear brick elements with reduced integration (C3D8R) with a nominal mesh size is 10 mm. Like for the bolts, some features and geometry are lost in the meshing, as illustrated in figure 13b with the meshed geometry in blue and geometrical model in red outline. Material properties are identical for bolt and washer and are shown in table 11.

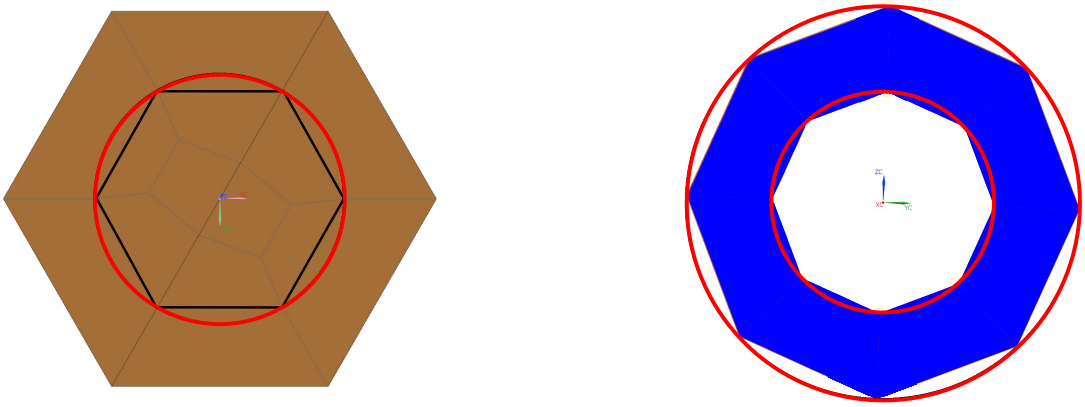

(a) Comparison between model and meshed bolt. (b) Comparison between model and meshed washer.

Figure 13: Comparison between modelled and meshed geometry.

Table 11: Bumax 109 (AISI 316L) material properties.

Material	Youngs's modulus $[GPa]$	Poisson's ratio	Density $[Kg/m^3]$	Thermal expansion coefficient K^{-1}	Fracture strain	Yield point 1 (stress strain) $[MPa, -]$	Yield point 2 (stress strain) $[MPa, -]$	Yield point 3 (stress strain) $[MPa, -]$
AISI 316L	210	0.3	7800	$1.1 * 10^{-5}$	0.078	1100 0	1674 0.011	1910 0.127

A.1.4 Vehicle model

The Norwegian Public Roads Administration supplied a complex LS-DYNA model of a Geo Metro compact type vehicle. Since the increment size in a dynamic explicit type simulation is directly related to the smallest element size in the model, simplifications were performed to reduce simulation time [14]. One such simplification was to remove the wheel knuckles and replace them with lumped masses of the same weight. The initial weight of the vehicle was 788 kg, which is lower than specified in the standard[7]. To make the mass of the vehicle comply with the weight requirement of the standard, a lumped mass of 100 kg, which is the maximum allowed ballast, was added to the vehicle. The lumped mass was added to an *MPC control point*, distributing the weight in the center of the vehicle causing no significant alteration of the CoG. The placement of the point mass is shown in figure 14 with green square being the point mass and purple being the *MPC connector*. The LS-DYNA model of the vehicle contained more than 200 different materials that were imported into the Abaqus model; these will not be covered here. The model consists of three different types of mesh, namely linear four node shell elements (S4R), linear triangular shell elements (S3R) and linear brick elements (C3D8R) with a mesh size between 18 and 77 mm. The vehicle is shown in figure 15.

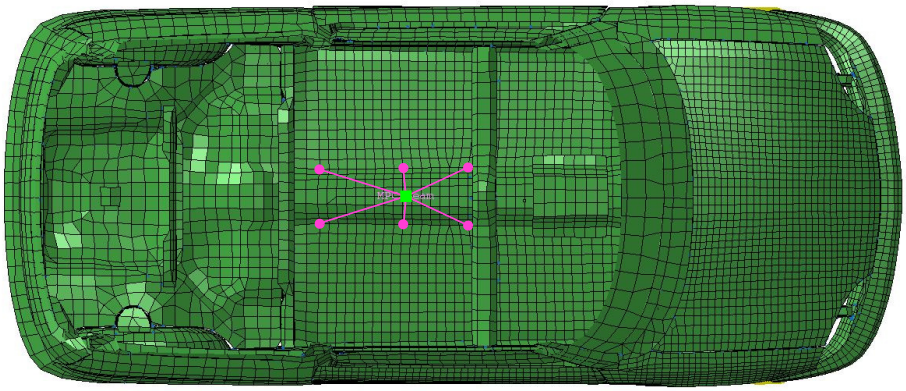

Figure 14: Location of the added vehicle mass

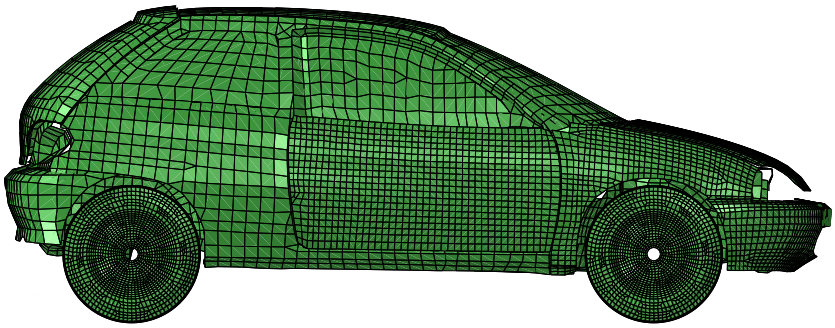

Figure 15: Simplified GM compact

A.1.5 Sign

The signs in the model are made from the same aluminum as the mast and modeled as a 3D shell. Mid surface was used to get the desired thickness of 4.15 mm. For additional strength, ribs were added for each 0.4 m horizontally as well as two vertical ribs, as shown in figure 16. The sign is meshed using linear shell elements with reduced integration (S4R) with a mesh size of 20 mm.

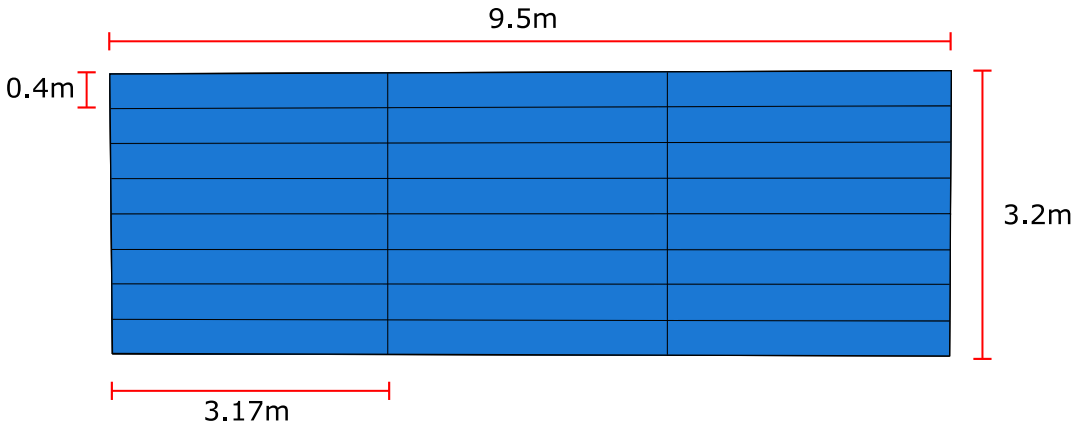

Figure 16: The sign with measurements

A.1.6 Simplified gantry

For the simplified model, a large section of the gantry was represented with beam elements. An iterative process was used to obtain equivalent material properties for the beam elements and the fully modeled mast [14]. The resulting section is shown in figure 17 and material properties in table 12. The different parts of the gantry are connected using a *coupling* type constraint with standard configuration, meaning the parts are constrained in all degrees of freedom relative to each other. As the simplified model has two center masts for additional support, two *coupling* constraints were used to connect the two vertical and the horizontal beam sections. One is linking the two vertical, and the other is connecting the horizontal *coupling* element to the transom. In figure 18, the black lines represent the beam elements of the gantry with yellow lines representing

coupling constraints. The 3D modelled mast is connected to the far right of figure 18.

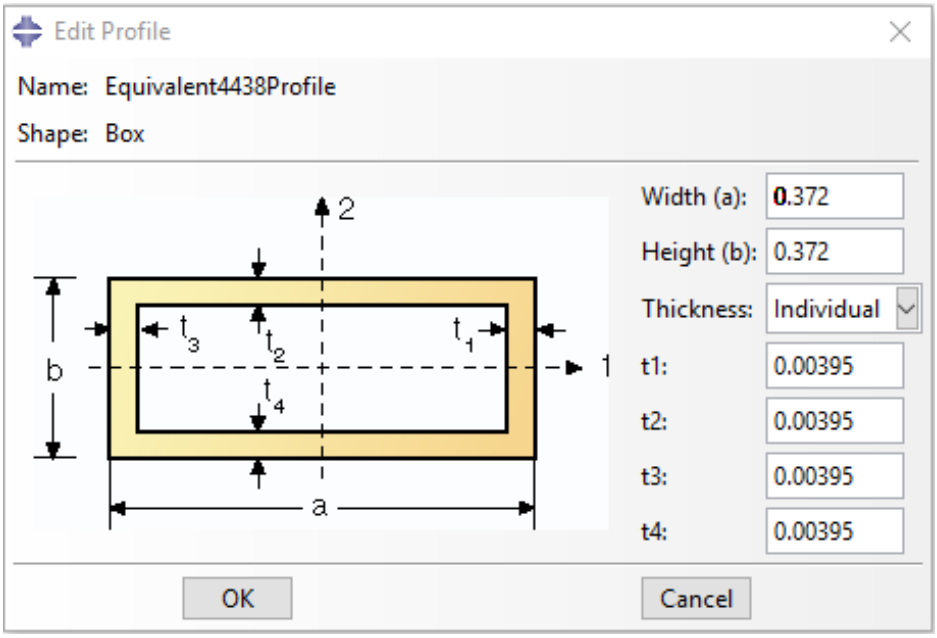

Figure 17: The profile of the beam elements in the gantry.

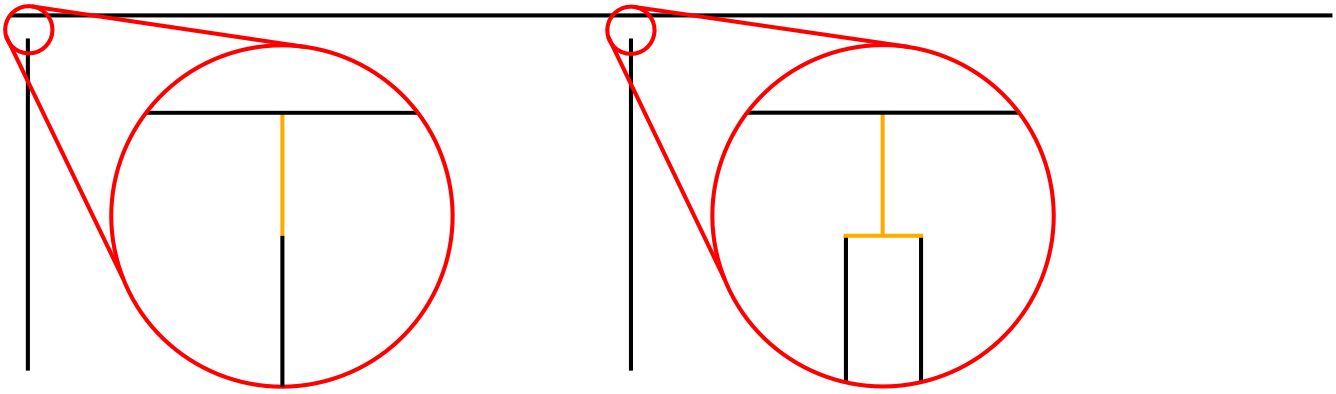

Figure 18: The beam elements making up the gantry with detail sections of the connections.

Table 12: Material properties of the tuned aluminum used for the gantry.

Material	Young's modulus $[GPa]$	Poisson's ratio	Density $[Kg/m^3]$
Tuned aluminum	59.9	0.275	3584.6

A.1.7 Bracket

The bracket is a design by Lattix, which is easy to manufacture and install. When the vehicle impacts the base of the support leg, the bracket is subjected to a large bending moment, consequently shearing the M10 bolts and separating the support leg from the transom. An exploded view of the bracket is shown in figure 19 along with figure 20 showing the shearing movement.

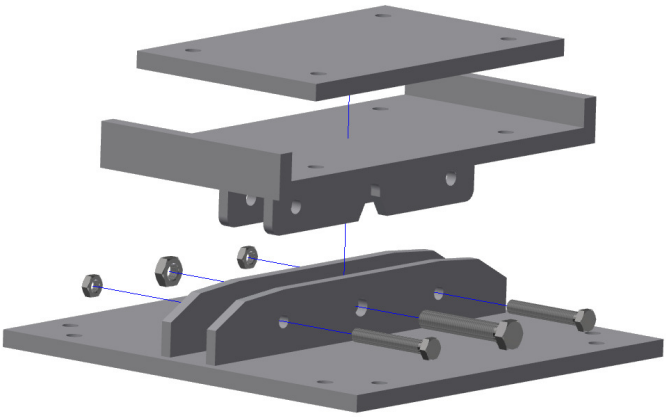

Figure 19: Exploded view of the shear bracket

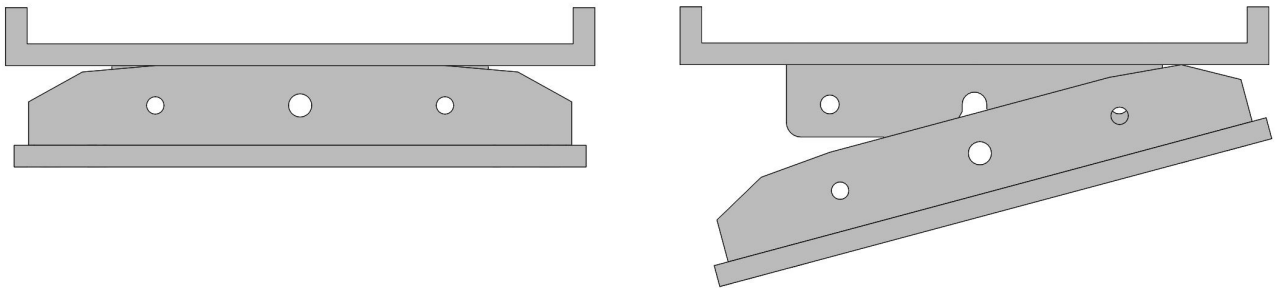

Figure 20: Failure mode of shear bracket

A.2 Assembly

A.2.1 4438 mast

The mast consists of three parts: mast start module, mast center module, and base plate. A *tie constraint*, shown in orange in figure 21a, connects the mast sections in touching surfaces while the base plate is bolted to the mast. These are notched bolts designed to break on impact. Figure 21b shows a cross-section of the bolted connection, where the bolts are shown in blue, washer in red, base plate in gray and mast in green. Abaqus does not allow for the importation of more than one assembly. Since the vehicle is the most complex part, it was decided to use this as the assembly, and hence the mast assembly had to be imported as a part. An assembly imported as a part is

not as easily modifiable, and changes to the mast require the original assembly to be altered and re-imported.

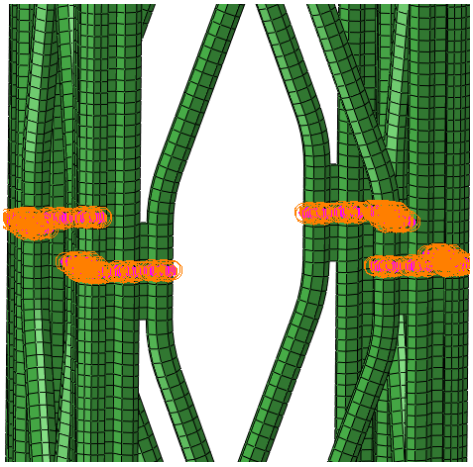

(a) *Tie connection* of the mast sections.

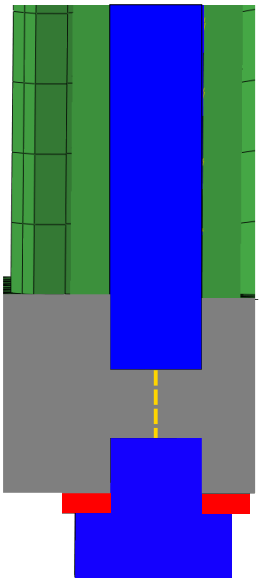

(b) Section view of bolt connection to base plate.

Figure 21: The joining of Lattix 4438 mast parts.

Figure 22: Fully assembled Lattix 4438 mast.

A.2.2 Complete gantry

The complete gantry was made using the Lattix 4438 masts for all vertical legs, and mast center modules in a series for the transom. These parts replaced the beam elements formerly used as the gantry. The legs of the gantry were made using *linear pattern* with the initial mast as the origin. As the distance between the mast legs is unequal, one was first placed and then used as an origin for the last. The first section of the transom was placed and then *linear pattern* was used to get the desired length. Unlike the simplified model, only one center mast was used for the full model. The reason for this was to reduce installation cost, and this change in the number of center masts was expected to have a negligible influence on ASI and THIV.
Two signs are mounted on the transom, one for each lane direction. The signs are identical and placed in between the gantry legs symmetrical around the transom. Figure 23 shows the full model of the gantry with measurements showing the placement of the different parts.

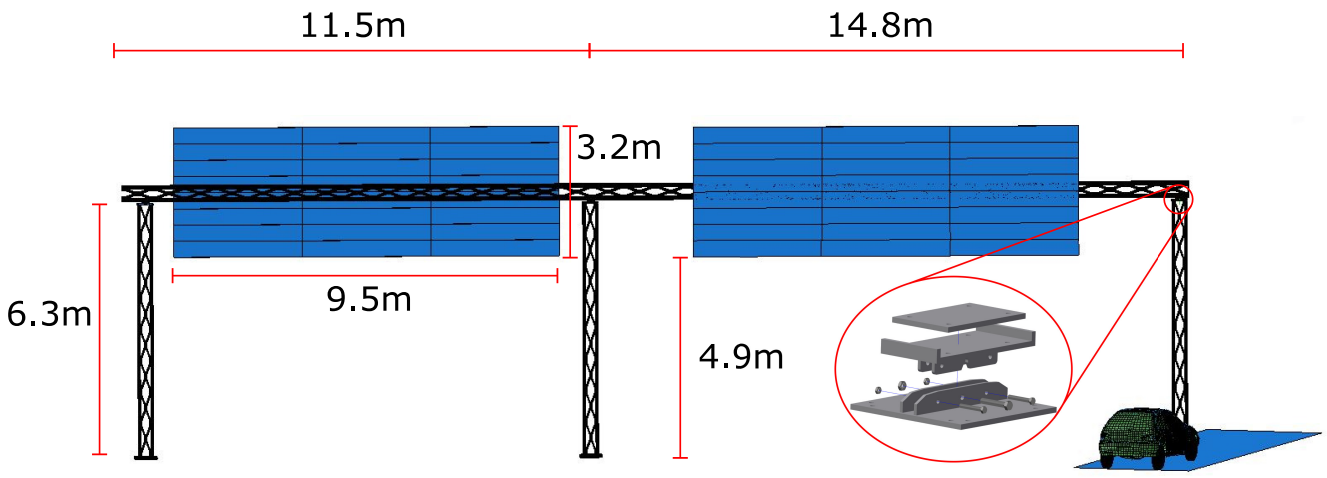

Figure 23: Full gantry

A.2.3 Positioning of the vehicle relative to the mast

The vehicle is given initial velocity in the first step, "Initial", and starts moving in the following step, "Pretension". For the vehicle not to hit the mast before the bolts have been adequately pre-tensioned, it has to be positioned at a distance from the mast. This distance depends on the time it takes to pre-tension the bolts and the velocity of the vehicle. The required distance between the vehicle and the mast was calculated using equation (5) and the resulting distances are shown in table 13. The reason for what appears to be an unnecessarily large distance for the lower velocity is trial and error. When placing the vehicle closer to the mast, contact between vehicle and mast had already occurred by the first frame in "Crash". To ensure that no contact is made between the vehicle and mast before bolts are adequately pre-tensioned it was decided to increase the distance between vehicle and mast to 0.0025 m

$$x_{min} = v_{initial} * t_{pretension} \tag{5}$$

Table 13: Distance between vehicle and mast for the different velocities.

Initial velocity $[km/h]$	Minimum distance, x $[m]$	Distance in model $[m]$	Time to impact $[s]$
100	0.00278	0.00465	$1.674 * 10^{-4}$
35	$9.72 * 10^{-4}$	0.0025	$1.54 * 10^{-4}$

The mast was placed directly in front of the vehicle with an angle θ of 20° with the Y-axis of the vehicle, and the impact point is 51mm in the positive Y direction from the center axis of the vehicle. At the top, the mast is connected to the transom following the same 20° angle with the Y-axis. The position of the vehicle for 100 km/h is shown in figure 24, the black center line

representing the center axis of the vehicle, black vertical line parallel to the Y-axis and the red line is the center line of the transom.

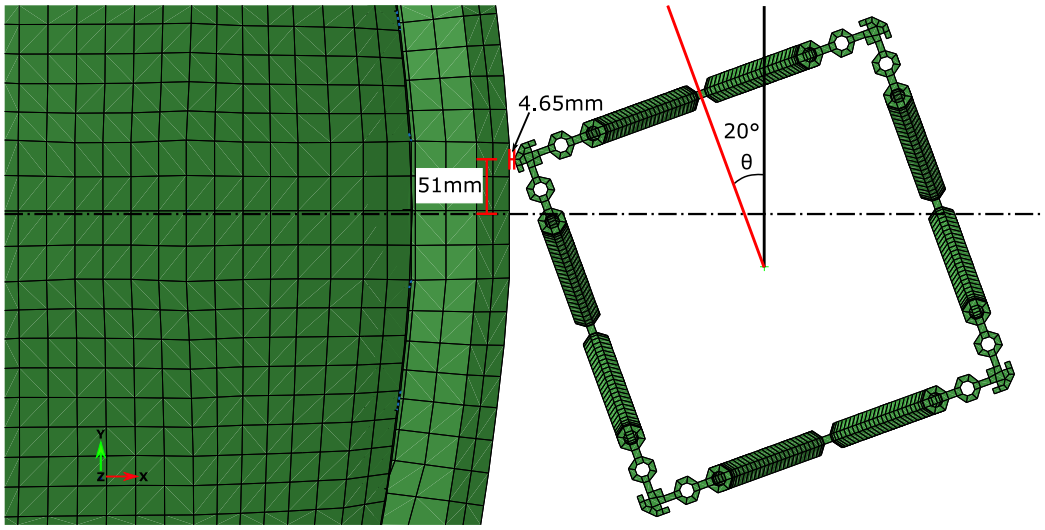

Figure 24: The positioning of the vehicle relative to the mast.

A.3 Interaction

A.3.1 Interactions

There are two different interactions defined in the model. As large displacements are expected in crash simulations, there is a need for contact definition when deformation causes contact between surfaces. Such a contact will induce friction between these surfaces, and this friction must be defined. This contact was defined with a *general contact* that involves all exterior surface, edges, beam segments, and rigid surfaces. The friction within the model itself is defined with a friction coefficient of 0.1 (right in figure 25). Because of different friction needed in the model, there are two exceptions from the *general contact* shown on the left in figure 25. The first surface is where the tires are in contact with the road as it would be in real life (figure 26). This contact is defined as frictionless to remove any resistance from the road to tire contact (figure 27) as this is applied as a load. The other exception is between the bracket and top of the mast.

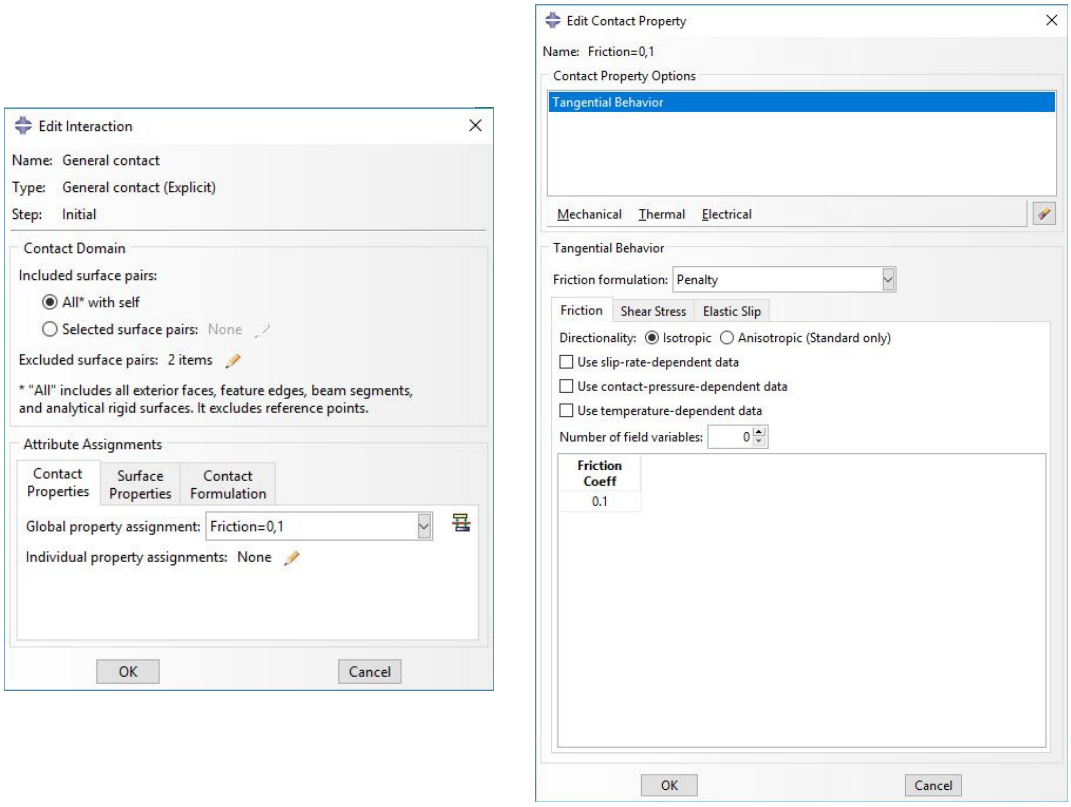

Figure 25: General contact and contact properties

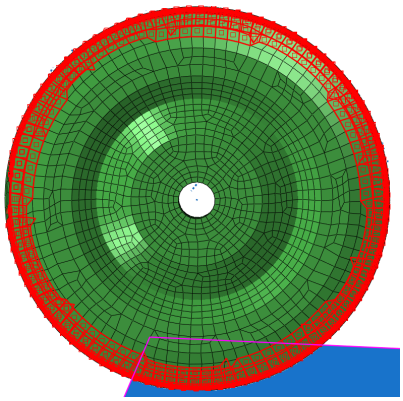

Figure 26: Nodes for the contact definition between tire and road.

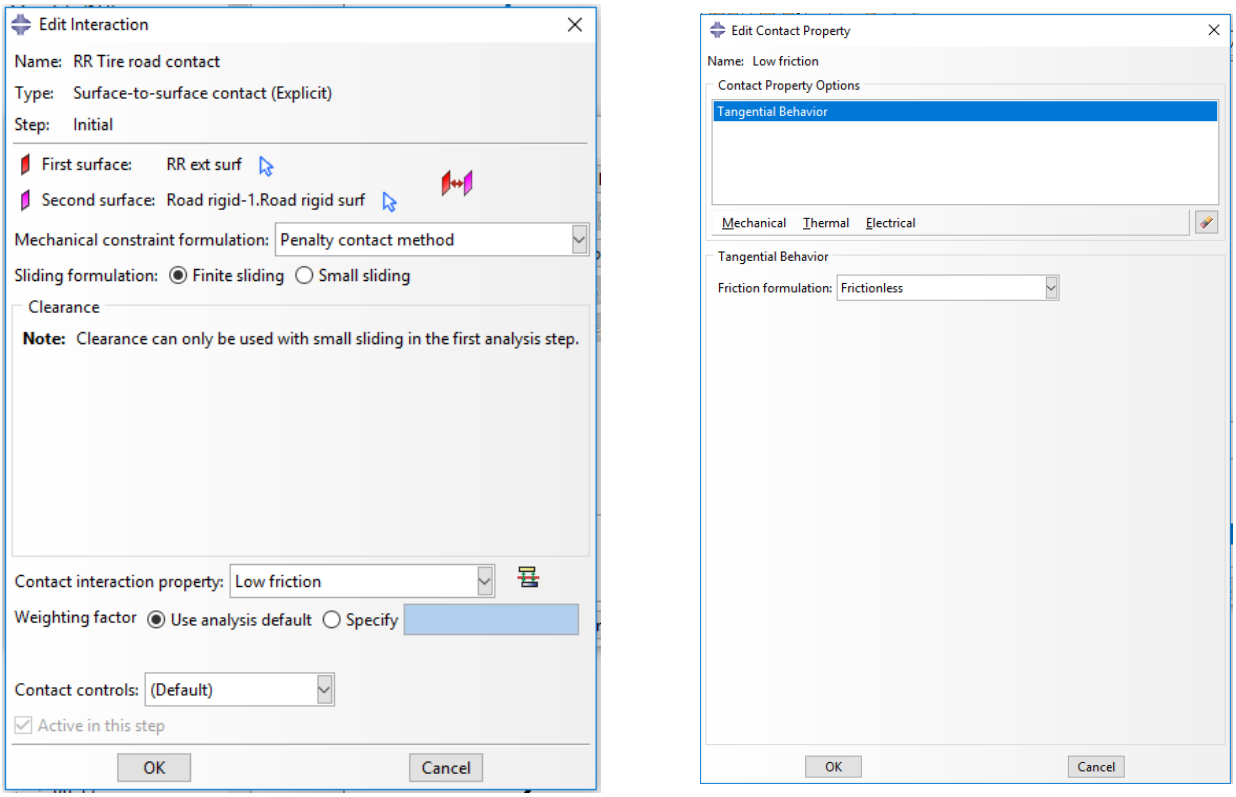

(a) Contact definition between road and tire.

(b) Frictionless contact.

Figure 27: Contact definition between road and tire.

A.3.2 Transom and sign

The transom is connected using multiple *tie constraints* between the different sections. No joints are present in the transom as this was considered having minimal impact on the results, but would increase simulation and modeling time.
The signs are also connected to the transom using *tie constraints* in the coincident surfaces. In this constraint, the signs are the master surface and transom the slave as the signs have the coarser mesh [25]. The adjustment of slave nodes was turned off.

A.3.3 Top wire connector

For the simplified model, a wire connector was used to connect the 3D modeled leg to the beam element transom, as shown in figure 28. This connector is a simplification of a frangible connection. The fracture load of this connector is what affects the results with regards to ASI and THIV for initial simulations where the fracture load of the lower bolts is not changed. The connection point on the top of the mast is made with an *MPC constraint* connecting the entire top section, as shown in figure 29 with the center line of the transom in red. From the master point of the *MPC constraint*, the wire connector is connected to the endpoint of the transom represented with beam elements.

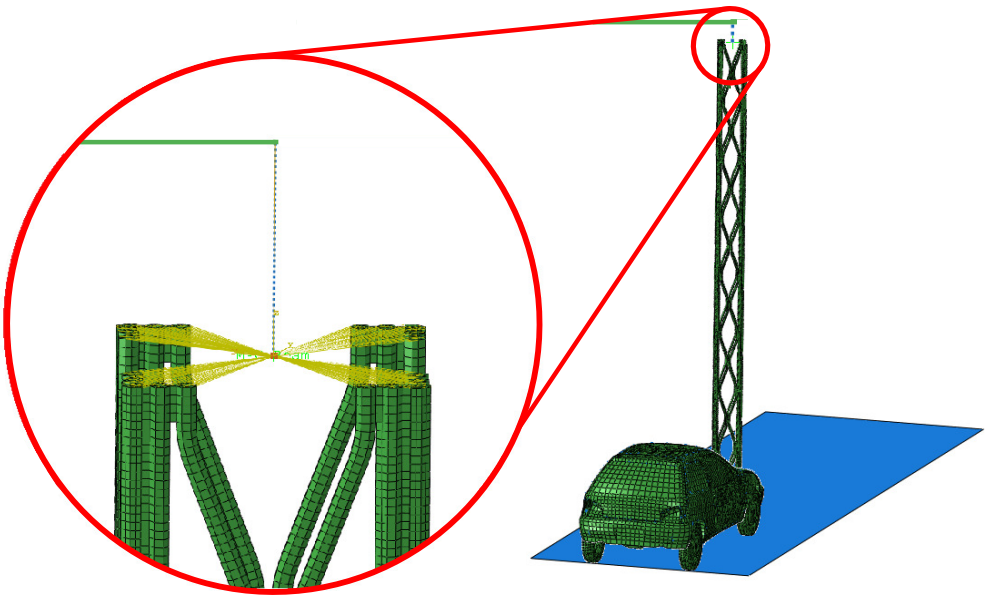

Figure 28: Location and detail figure of wire connector.

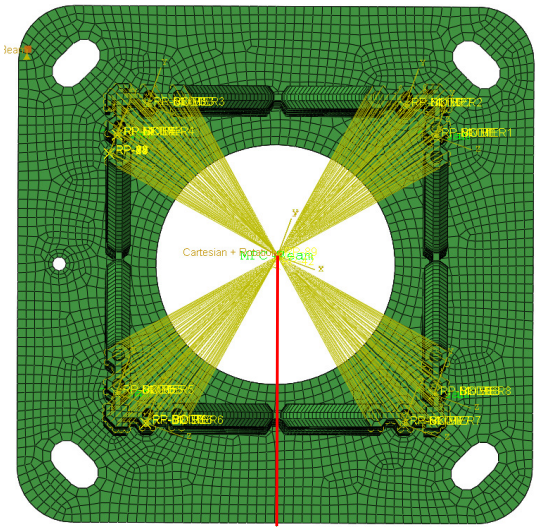

Figure 29: *MPC constraint* at the top of the mast.

A.3.4 Bolts

The bolts connecting the mast to the base plate are modeled as simplified frangible bolts. This connection was made by removing the section of the bolt where the notch would be and replacing it with a wire connector. The wire connector is connecting two *MPC constraints* with the center point of the cross-section as the master nodes. This wire connector is an *axial connector* type with failure criteria matching the desired failure load of the bolt (figure 30). The head section of

the bolt rests against the bottom side of the base plate, while the threaded section of the bolt is connected to the mast using *MPC constraints*. The connection between bolt and mast is shown in figure 31, with a red ring around the fracture section with the connector.

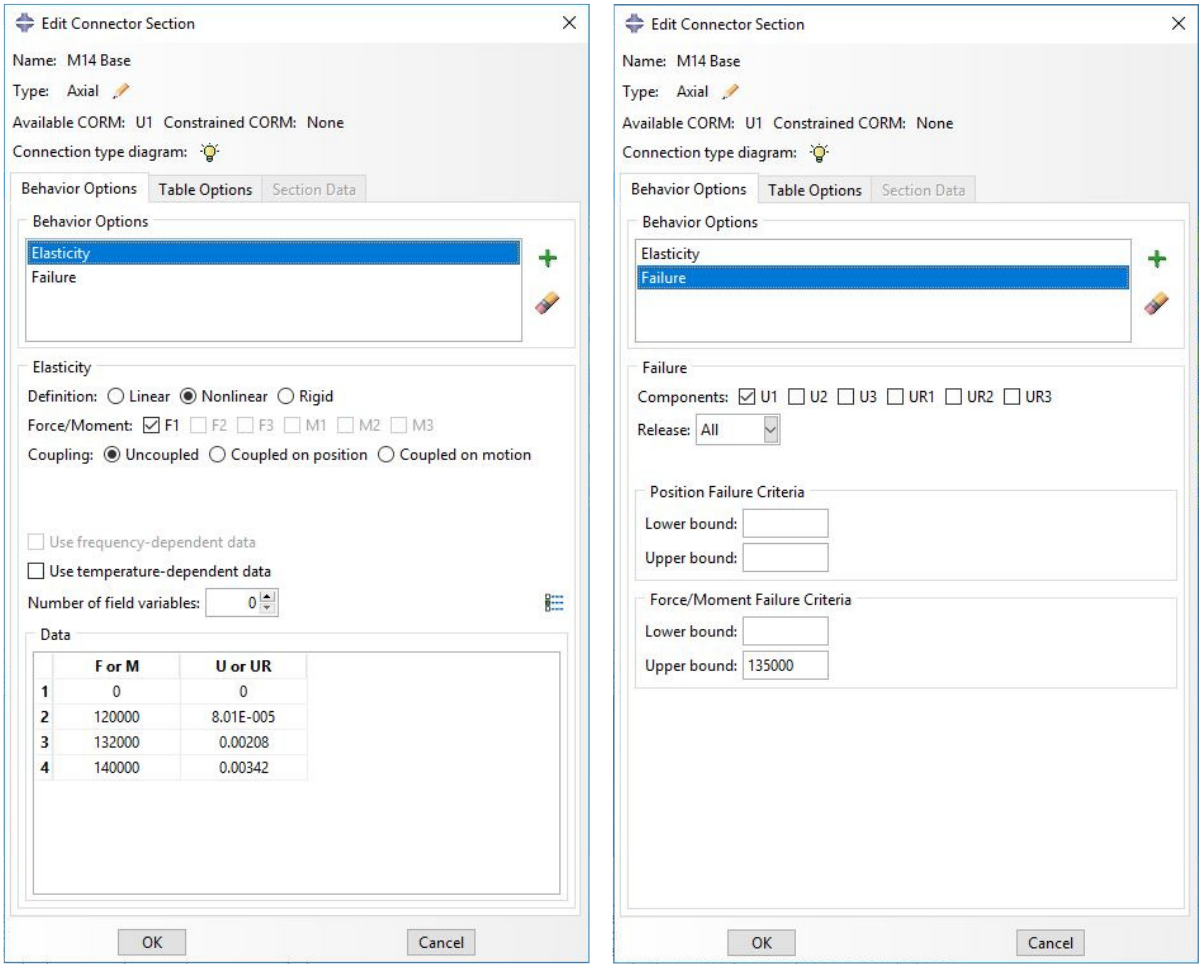

Figure 30: Elastic and fracture load of connector

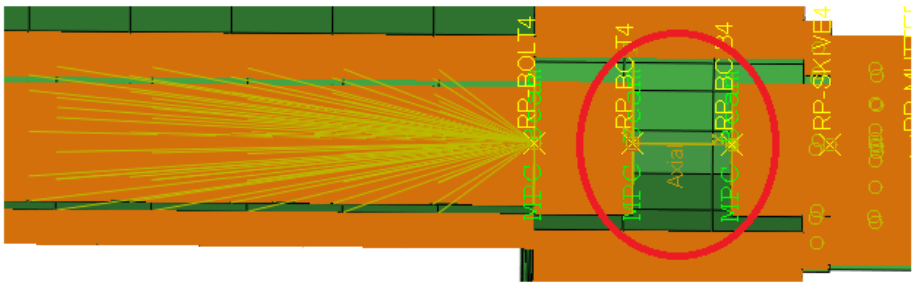

Figure 31: Section view of a bolt.

A.3.5 Bracket wire connectors

A simplification was done for the shear bracket by replacing the bolts with wire connectors with defined fracture load. This simplification was done somewhat different from the other bolt simplifications in the model. Instead of using wire connectors between two bolt sections, the entire bolt was replaced with wire connectors. The replacement was done using an *MPC constraint* to the center of the bolt holes and then connecting these with wire connectors. For the physical part, two long M10 bolts are meant to be used. In the model the wire connectors represent four short bolts instead of two long, meaning a total of four wire connectors are used. Both the *MPC constraint* and the bolt simplification are shown in figure 32 with yellow being the *MPC constraint* and red being the wire connector.

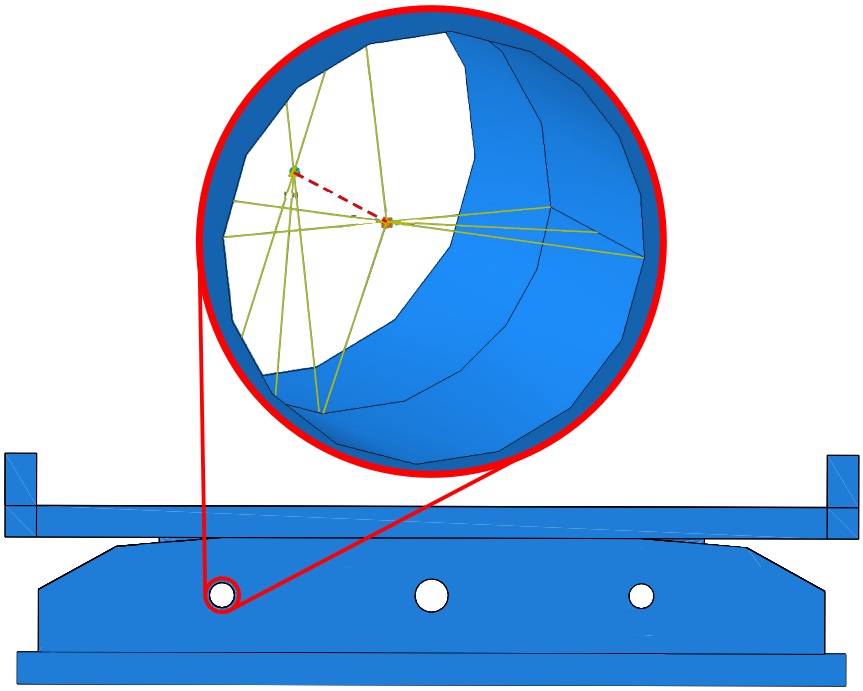

Figure 32: Bracket with detailed view of connector and MPC connection

A.4 Boundary conditions

A.4.1 Initial velocity

Initial velocity is defined using *predefined field*. The *predefined field* is defined in the initial step on all the nodes in the vehicle; body, wheels, and reference points. Impact between vehicle and mast happens in the crash step since the necessary distance between the vehicle and the mast is ensured so that pretension of the bolts are allowed to finish. The velocity is either 100 km/h (27.78 m/s) or 35 km/h (9.72 m/s), depending on the case, in positive x-direction. Figure 33 shows the setup of the initial velocity of the vehicle.

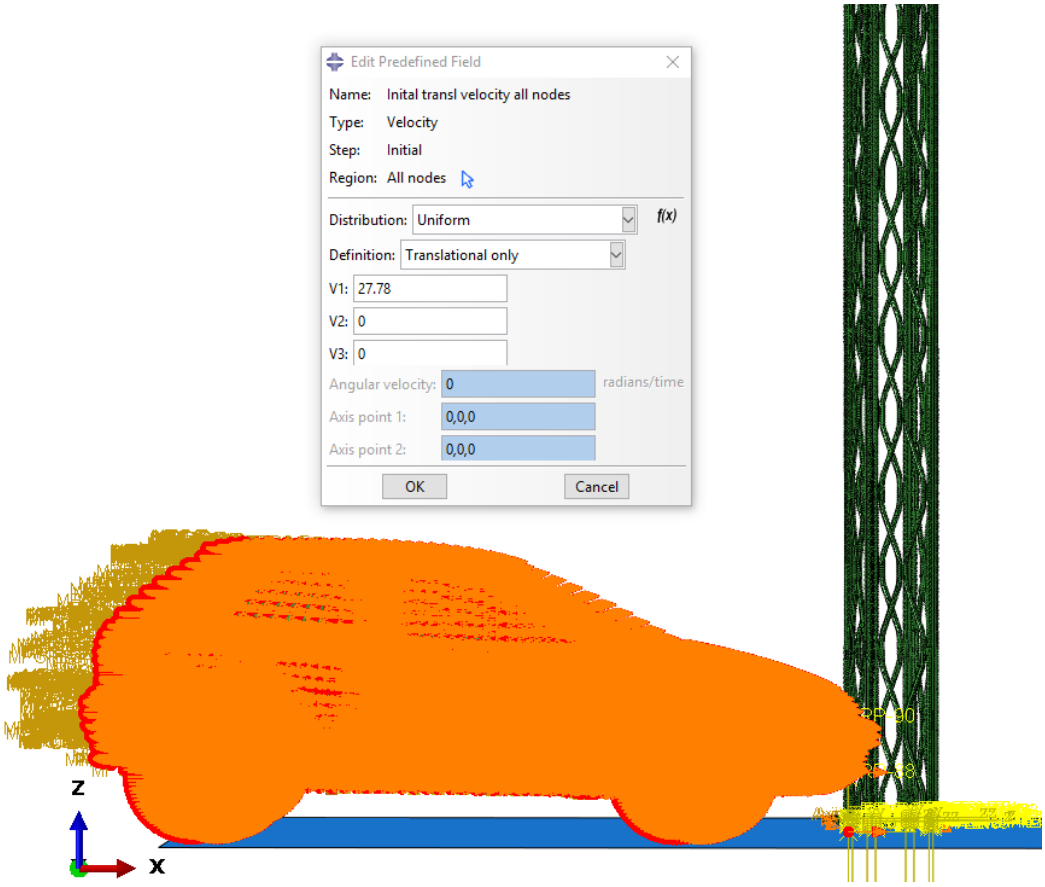

Figure 33: Setup of the initial velocity

A.4.2 Rolling resistance

To mimic the rolling resistance the vehicle would have, a load is applied to the node set "Rolling rest points" consisting of four center nodes of the *MPC constraint* on the inside of the tire. These nodes are located at the central point of the hinge connector between the wheels and vehicle, as shown in figure 34. A force of -250 N is applied in X direction working against the movement of the vehicle.

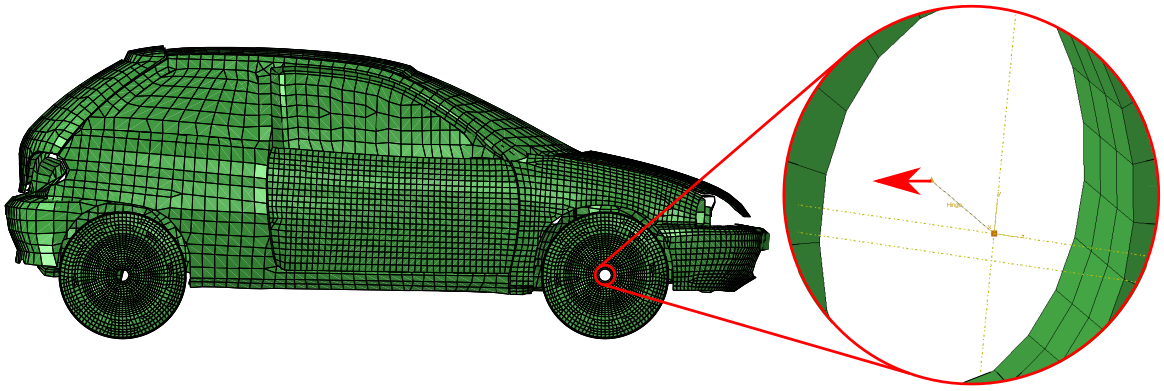

Figure 34: Rolling resistance of the vehicle.

A.4.3 Gravity

Gravity load was applied to the whole model, meaning all parts of the assembly is subjected to an acceleration in negative z-direction equivalent to 1g ($-9.81 m/s^2$). The gravity load is applied in the pretension step.

A.4.4 Bolt pretension

The pretension of the bolts connecting the mast to the base plate is made utilizing thermal expansion of the material at a change in temperature. To achieve the desired pretension, an initial temperature of 273.15 K was defined (figure 35a). To achieve pretension, the bolt needs to shrink, meaning ΔT needs to be negative. The exact value for ΔT was found through iteration[14].

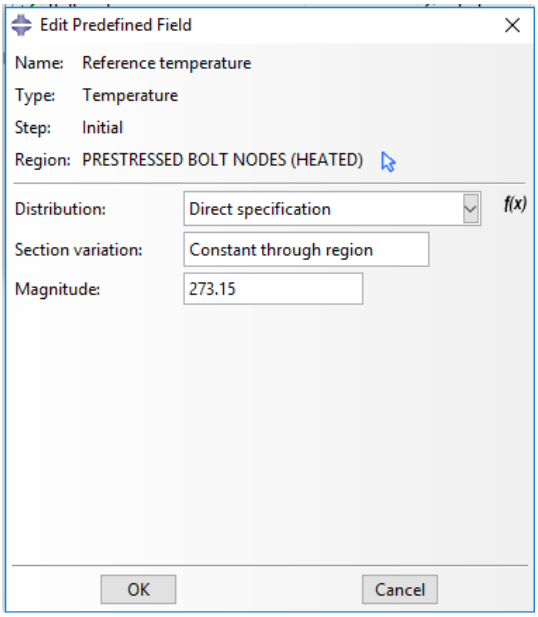

(a) Initial temperature.

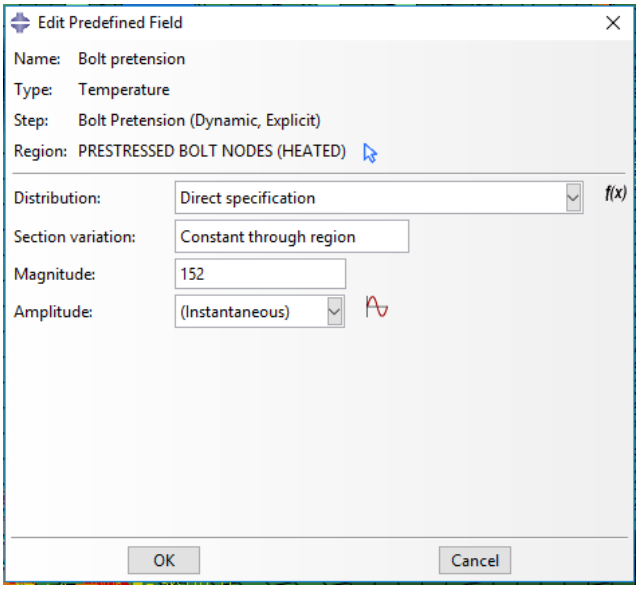

(b) Required temperature to obtain desired pretension.

Figure 35: Setup of the *predefined* field giving pretension in the bolts.

B Complementary results

B.1 Crash

Figure 36: Deformation in vehicle, mast, and transom

Figure 36 shows the deformation in the vehicle, mast and transom during the crash step with the right frames being the transom. The top two frames show the initial step where the vehicle has yet to make contact with the mast — no deformation in either base or top as expected. For the middle frames, it is clear that all the bolts have failed as intended and severe deformations in the mast have occurred. Despite large strains at the base, little of this deformation can be observed in the transom. Some stress can be seen in the bolt holes, but the connectors are still intact. In the bottom frames, the mast is moved free of the base plate and induces more moment into the upper bracket. This increase in load is shown by the higher stresses in the bolt holes. The bolt holes are no longer concentric showing that the connectors have failed, meaning the upper and lower part of the bracket are no longer connected. With the bolts, both top and base, fractured the mast is no longer connected to anything and moving freely with the vehicle as can be seen in figure 37.

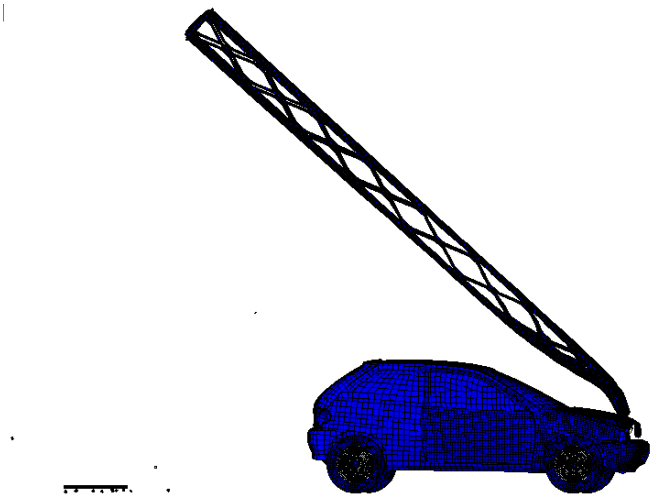

Figure 37: Last time step of simulation

The final deformation of the transom at the end of the simulation, at 275 ms, can be seen in figure 38 with a green square showing initial and a red square showing the final position. The torsion load for the long transom section is 18.7 kNm, and 14.4 kNm for the short section. The torsion capacity of the transom is 21 kNm. No factor of safety or material factor have been included in the torsion calculations. If the torsion in the transom increases, the long section of the transom may have torsion loads above allowable limits. The signs are expected to reduce the torsion to some degree because of the resistance of air, but not enough to decrease the torsion load drastically. An issue is that the behavior of the transom after the end of the simulation is unknown.

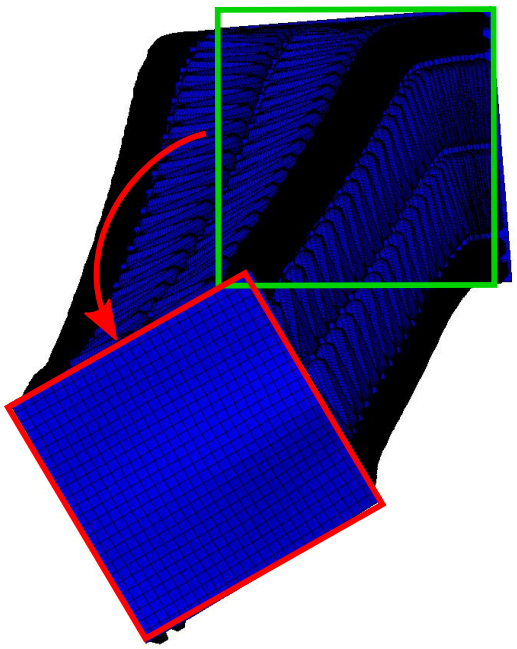

Figure 38: Deformation in transom

B.2 Wind load

Initial wind simulations with one center mast were done using body loads. For these simulations, the relationship between applied load and displacement in the transom is no longer linear after 67.5 kN, indicated with the red line in figure 39a. At this point, the structure starts to yield severely, and the risk of complete failure increases drastically. This was also shown when the body load was replaced with a pressure load applied to the sign. These simulations were aborted before completion, and visual inspection of the cross-section shows that yielding in the cross-section starts at 1 kN/m^2 which is equivalent to 60.8 kN, shown with the grey line in figure 39a. Because of the lack of completion, there is no apparent deviation in the relationship between applied load and displacement in the transom for pressure load, but it shows signs of starting to curve at the end which corresponds well to the start of the curvature in the body load graph, as expected.
For the double mast configuration, the strength of the structure is significantly increased. Unlike the single mast configuration, the body load simulation failed before completion, and the pressure simulations were completed. The pressure load graph starts to curve at 1.5 kN/m^2, which corresponds to 91.2 kN. This curvature is not observable for the pressure load, and the reason for this is unknown. Visual verification indicates that the center masts starts to yield at 1.4 kN/m^2, which corresponds to 79 kN.
Analytic calculations of the bending capacity yield different results than the simulations with a maximum wind load of 0.79 kN/m^2 for single and 1.58 kN/m^2 for double center mast. Using the conservative findings, the structure with this exact sign configuration can be classified as WL2 and WL7 for single and double center mast respectively. Exact calculations according to standards[13, 12, 17] are necessary when the geometry of the structure and geographical location are determined.

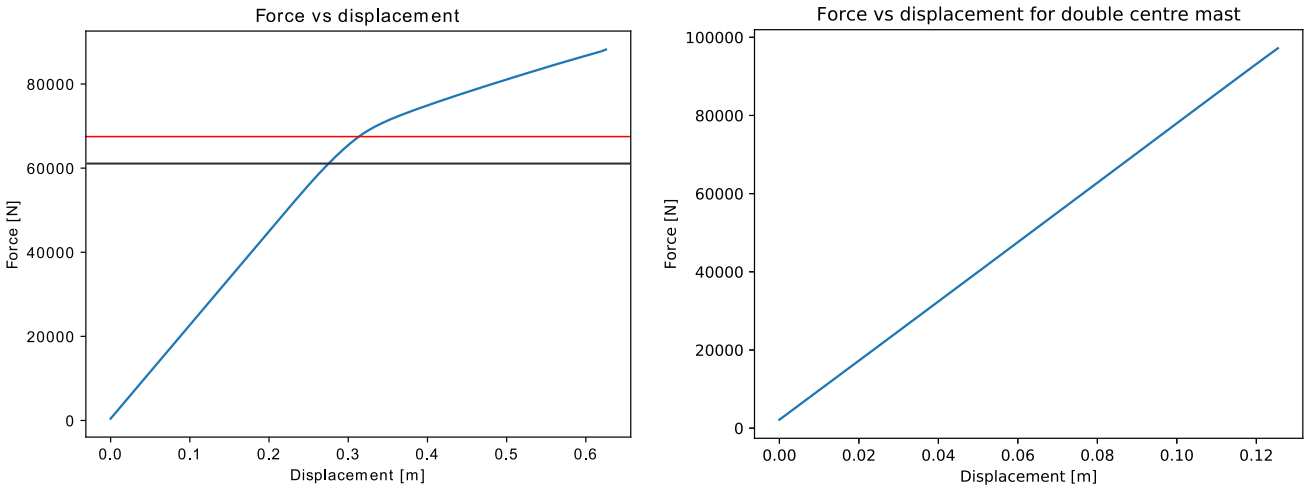

(a) Single mast configuration

(b) Double mast configuration

Figure 39: Applied body load vs displacement of transom for both configurations

B.3 Combined load simulation

A simulation combining crash with wind load was performed to investigate if the gantry would withstand being crashed into in windy weather conditions. The standards do not demand such a test for being classified as a non-energy absorbing structure; however, it is a matter of traffic safety and based on the weather conditions in Norway the situation is not unlikely.
The addition of a wind load of 0.325 kN/m^2 has a neglectable impact on ASI and THIV values, at 0.51 and 10.1 respectively, compared to 0.50 and 10.4 without wind load. These results imply that there is no significant difference in occupant safety when crashing in windy weather.

When the wind already induces load onto the mast before the vehicle hits the structure, some of the material capacity of the base bolts is spent. This lowered capacity in turn lowers the ASI value because of the lower load needed to be applied into the structure by the vehicle. However, the gantry has been deformed by the wind and is leaning somewhat in the direction of the vehicle's movement. This leaning is suspected to increase ASI seeing the transom is being pushed upwards before dislocating from the mast. The two factors are working against each other resulting in small changes in ASI. It shall be noted that how much of an impact these two factors have isolated on the ASI value is unknown.

C Python scripts

Several Python scripts were made for post processing of simulation data. The most used scripts for data processing are presented here. The script exporting XY data is run from the Abaqus client, while the other two are run using Python IDE.

C.1 Extracting XY data from .odb

```
from abaqus import *
from abaqusConstants import *
from Tkinter import Tk
import os
import __main__


#input:
# The full path of the odb location with odb extension
LocationOfODB = 'C:/Users/torbjlaa/Abaqus_Simulations/35kmh100kg_135_22.odb'
# Desired name of files, stock name is ASIx, y, z, and THIV with a number behind.
    Can also be string but NO SPACES!
NumberInLine = "35kmh100kg_135_22"
# Desired saving location for text files
DataFileLocation = "C:/Users/torbjlaa/Documents/Python/ASI/"

#main code:
def main():
    label = ["x", "y", "z"]
    c = 0
    for i in label:
        c += 1
        odbName = session.viewports[session.currentViewportName].odbDisplay.name
        # defining desired step and frames
        session.odbData[odbName].setValues(activeFrames=(('Crash', ('0:-1',)), ('
    ASITing', ('0:-1',))))
        odb = session.odbs[LocationOfODB]
        # The construction of XY data where desired output and extraction point are
     defined
        session.xyDataListFromField(odb=odb, outputPosition=NODAL, variable=(('A',
    NODAL, ((COMPONENT, 'A{}'.format(c)),)),), nodeLabels=(('CAR-1', ('41395', )),))

        # create a Tk device and clear the current clipboard
        # constructing file for writing data with desired save location
        f = open("{}ASI{}_{}.txt".format(DataFileLocation, i, NumberInLine), "w+")
        r = Tk()
        r.clipboard_clear()

        # data from XY data added to variable
        for xyDataKey in session.xyDataObjects.keys():
            xyData = session.xyDataObjects[xyDataKey]
            # writing name of output with output point, eks A:A1 reference point 42
            print("copy {} to clipoard".format(xyDataKey))
```

```
            f.write("{}\n".format(xyDataKey))

            # writing acceleration data for all points to file
            for line in xyData:
                nline = "{}\t\n".format(line[1])
                f.write(nline)

        # destroy tk device
        r.destroy()
        f.close()
        # deleting current xy data from xy data manager to allow for nesting of several XY
        del session.xyDataObjects['A:A{} PI: CAR-1 N: 41395'.format(c)]


#_____________________________________________________________________________
#THIV

    odbName = session.viewports[session.currentViewportName].odbDisplay.name
    # defining desired step and frames
    session.odbData[odbName].setValues(activeFrames=(('Crash', ('0:-1',)), ('ASITing', ('0:-1',)), ('After crash', ('0:-1',))))
    odb = session.odbs[LocationOfODB]
    # The construction of XY data where steps, frames, desired output and extraction point are defined
    session.xyDataListFromField(odb=odb, outputPosition=NODAL, variable=(('V', NODAL, ((INVARIANT, 'Magnitude'),)),), nodeLabels=(('CAR-1', ('41395',)),))

    # create a Tk device and clear the current clipboard
    f = open("{}THIV_{}.txt".format(DataFileLocation, NumberInLine), "w+")
    r = Tk()
    r.clipboard_clear()

    # copy xy data to clipboard
    for xyDataKey in session.xyDataObjects.keys():
        xyData = session.xyDataObjects[xyDataKey]

        print("copy {} to clipoard".format(xyDataKey))
        f.write("{}\n".format(xyDataKey))
        # writing both time steps and velocity
        for line in xyData:
            nline = "{}\t{}\n".format(line[0], line[1])
            f.write(nline)

    # destroy tk device
    r.destroy()
    f.close()
    # deleting current XY data from XY data manager to allow for nesting of several XY
    del session.xyDataObjects['V:Magnitude PI: CAR-1 N: 41395']


if __name__ == '__main__':
```

```
88      main()
```

C.2 ASI for moving average

```
from math import *
import matplotlib.pyplot as plt

# average values in list
def avrg(list):
    average = sum(list)/len(list)
    averageG = average/9.81
    return averageG


def main():

    # the path for text files containing raw XY data
    LocationOfFile = "C:/Users/torbjlaa/Documents/Python/ASI/"
    # number or name of the ASI file, ex 100kg_100kmh
    NumberOfFile = "35kmh100kg_135_22"

    # Reading raw XY data from x dir
    unmodX = open("{}/ASIx_{}.txt".format(LocationOfFile, NumberOfFile), "r")
    # Reading raw XY data from y dir
    unmodY = open("{}/ASIy_{}.txt".format(LocationOfFile, NumberOfFile), "r")
    # Reading raw XY data from z dir
    unmodZ = open("{}/ASIz_{}.txt".format(LocationOfFile, NumberOfFile), "r")
    # Generating results txt file
    Resu = open("{}/ASI_Total_{}.txt".format(LocationOfFile, NumberOfFile), "w+")

    Xu = unmodX.readlines()
    Yu = unmodY.readlines()
    Zu = unmodZ.readlines()
    ASIxMax = []
    ASIyMax = []
    ASIzMax = []
    Max = []

    # controlling the starting point for ASI calculations, starts with 0 to 2000,
    then 1 to 2001 etc
    for i in range(0, len(Xu)-2000):
        x = []
        y1 = []
        z = []
        # cycling through the 2000 data points equivalent to 50ms
        for y in range(1+i, 2001+i):
            point = int(y)

            # appending float value for x to x list
            x.append(float(Xu[point]))
            # appending float value for y to y list
            y1.append(float(Yu[point]))
            # appending float value for z to z list
            z.append(float(Zu[point]))

```

```
51          # making variable containing average of each component
52          xg = avrg(x)
53          yg = avrg(y1)
54          zg = avrg(z)
55
56          # checking components for individual criteria
57          ASIx = xg/12
58          ASIy = yg/9
59          ASIz = zg/10
60
61          # appending ASI for each direction to list
62          ASIxMax.append(ASIx)
63          ASIyMax.append(ASIy)
64          ASIzMax.append(ASIz)
65
66          # ASI criteria
67          ASItot = sqrt(ASIx**2 + ASIy**2 + ASIz**2)
68          # appending max ASI to list
69          Max.append(ASItot)
70
71      # determining max value in the list
72      valueTot = (max(Max))
73      # index for max value in list
74      indx = Max.index(valueTot)
75      # ASIx value for the specified index
76      valueX = ASIxMax[indx]
77      # ASIy value for the specified index
78      valueY = ASIyMax[indx]
79      # ASIz value for the specified index
80      valueZ = ASIzMax[indx]
81      # Time passed since crash step started in ms
82      MaxTime = indx * 0.025
83
84      # writing ASI for all direction and resulting ASI to txt file
85      Resu.write("ASI (x-dir): {} \nASI (y-dir) = {} \nASI (z-dir) = {} \nASI (Total)
        = {}\n"
86                 "Milliseconds since beginning of crash step = {}".format(valueX,
    valueY, valueZ, valueTot, MaxTime))
87
88      # printing max ASI to client
89      print(valueTot)
90      # Printing time passed since beginning of crash step
91      print(MaxTime)
92      # plotting max total ASI for each segment of the moving average
93      plt.plot(Max)
94      # showing the graph
95      plt.show()
96      # closing results file
97      Resu.close()
98  if __name__ == '__main__':
99      main()
```

C.3 THIV calculations

```
from math import *

#input:
# Input the name of the file here
filename = "35Final"
# location of the file, full path required
location = "C:/Users/torbjlaa/Documents/Python/ASI/"

NameOfFile = "THIV_{}.txt".format(filename)
# Result file gets the name of the filename + Results
NameOfResult = "THIV_Result_{}.txt".format(filename)

#Main code follows
def main():
    # initial time
    t = [0]
    # initial velocity, change when altering in simulation!
    v = [9.72]
    # initial head position
    x = [0]
    kmt = []
    r = []
    # range for head wander
    lower = 0.595
    upper = 0.61
    # Opening THIV file
    unmod = open("{}{}".format(location, NameOfFile), "r")
    # generating results file
    tot = open("{}{}".format(location, NameOfResult), "w+")
    lines = unmod.readlines()

    # cycles through lines in THIV file, splits time steps and velocity
    for i in range(1, len(lines)):
        # separating time and velocity
        r.append(lines[i].split("\t"))
        # Time steps appended to Time list
        t.append(float(r[i-1][0]))
        # Velocity appended to speed list
        v.append(float(r[i-1][1]))

    deltaV = 0
    # calculating head travel for all time steps using midpoint rule
    for i in range(1, len(t)):
        deltaV2 = v[0] - v[i]
        x1 = x[i-1] + (((deltaV + deltaV2)/2) * (t[i] - t[i-1]))
        # appending head travel to distance list
        x.append(x1)
        deltaV = v[0] - v[i]

    # converting m/s to km/h
    for i in range(len(v)):
```

```
52          kmt.append(v[i]*3.6)
53
54      indx = 0
55      c = 0
56      for i in x:
57          # checking all values of x to check if head has traveled 0.6m
58          if lower < i and i < upper:
59              # storing index for when head have traveled 0.6m and breaks the loop
60              indx = c
61              break
62          c += 1
63
64      # calculating relative speed of the head when hitting dashboard
65      vrelative = (v[0]*3.6) - kmt[indx]
66
67      # writing results to file
68      tot.write("THIV value when distance traveled by head = {}m: {}".format(x[indx],
        vrelative))
69      print("THIV value when distance traveled by head = {}m: {}".format(x[indx],
        vrelative))
70      tot.close()
71      return vrelative
72
73  if __name__ == '__main__':
74      main()
```

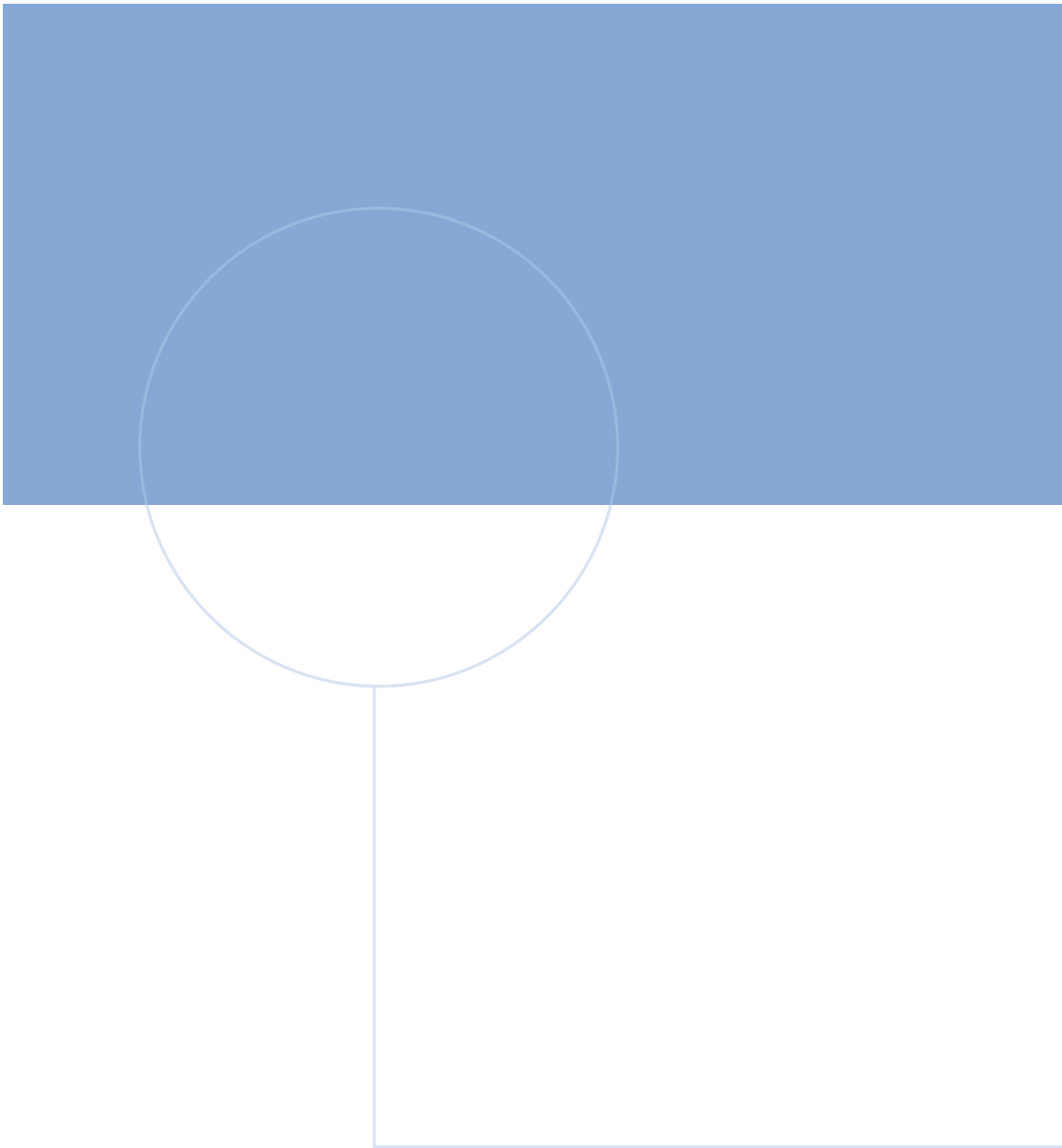

NTNU
Norwegian University of
Science and Technology